Targeting the Pregnane X Receptor Using Microbial Metabolite Mimicry

Zdeněk Dvořák[1]‡*, Felix Kopp[2]‡, Cait M. Costello[17], Jazmin S. Kemp[17], Hao Li[3]‡, Aneta Vrzalová[1]‡, Martina Štěpánková[1], Iveta Bartoňková[1], Eva Jiskrová[1], Karolína Poulíková[1], Barbora Vyhlídalová[1], Lars U. Nordstroem[2], Chamini Karunaratne[2], Harmit Ranhotra[3, $], Kyu Shik Mun[5], Anjaparavanda P. Naren[5], Iain Murray[6], Gary H. Perdew[6], Julius Brtko[7], Lucia Toporova[7], Arne Schon[8], Bret Wallace[9], William G. Walton[9], Matthew R. Redinbo[9], Katherine Sun[10], Amanda Beck[4], Sandhya Kortagere[11]*, Michelle C. Neary[12], Aneesh Chandran[13], Saraswathi Vishveshwara[13], Maria M. Cavalluzzi[14], Giovanni Lentini[14], Julia Yue Cui[15], Haiwei Gu[16], John C. March[17], Shirshendu Chaterjee[18], Adam Matson[19], Dennis Wright[20], Kyle L. Flannigan[21], Simon A. Hirota[21], Sridhar Mani[3,*]

[1] From the Department of Cell Biology and Genetics, Palacký University, Olomouc 78371, Czech Republic; Departments of [2] Biochemistry, [3] Medicine, Genetics and Molecular Pharmacology, and [4] Pathology of The Albert Einstein College of Medicine, Bronx, NY 10461, USA; [5] Cincinnati Children's Hospital Medical Center, Cincinnati, OH 45229; [6] Department of Veterinary and Biomedical Sciences, Penn State College of Agricultural Sciences, University Park, PA 16802, USA; [7] Institute of Experimental Endocrinology, BMC, Slovak Academy of Sciences, Dúbravská cesta 9, 845 05 Bratislava, Slovac Republic; [8] The Department of Biology, Johns Hopkins University, Baltimore, MD 21218, USA; [9] Department of Chemistry, University of North Carolina, Chapel Hill, NC 27599; [10] The Department of Pathology, New York University School of Medicine, New York, NY 10016; [11] The Department of Microbiology and Immunology, Drexel University College of Medicine, Philadelphia, PA 19129 USA; [12] Department of Chemistry, City University of New York-Hunter College, New York NY 10065; [13] Molecular Biophysics Unit, Indian Institute of Science, Bangalore 560012, India; [14] Department of Pharmacy – Pharmaceutical Sciences, University of Bari Aldo Moro, Bari 70125, Italy; [15] Department of Environmental and Occupational Health Sciences, University of Washington, Seattle, WA 98105; [16] Center for Metabolic and Vascular Biology, College of Health Solutions, Arizona State University, Scottsdale, AZ 85259; [17] The Department of Biological and Environmental Engineering, Cornell University, Ithaca, NY 14853; [18] Department of Mathematics, City College of The City University of New York, NY, NY 10031; [19] Department of Pediatrics and Immunology, University of Connecticut, Farmington, CT 06030; [20] Department of Pharmaceutical Sciences, University of Connecticut, Storrs, Connecticut 06269-3092; [21] Department of Physiology and Pharmacology, University of Calgary, Calgary, AB Canada T2N 4N1

[$] Present Address: St. Edmund's College, Shillong, Old Jowai Road, Shillong, Meghalaya 793003, India

‡ Equal Contribution * Correspondence and requests for materials should be addressed to Z.D; S.K or S.M: (email: sridhar.mani@einstein.yu.edu)

KEYWORDS: Pregnane X Receptor, microbial metabolite, mimics, drugs, therapy, xenobiotic receptors, tryptophan, indole, indole propionate

Abstract

The human pregnane X receptor (PXR), a master regulator of drug metabolism, has important roles in intestinal homeostasis and abrogating inflammation. Existing PXR ligands have substantial off-target toxicity. Based on prior work that established microbial (indole) metabolites as PXR ligands, we proposed microbial metabolite mimicry as a novel strategy for drug discovery that allows to exploit previously unexplored parts of chemical space. Here we report functionalized indole-derivatives as first-in-class PXR selective non-cytotoxic agonists, as a proof-of-concept for microbial metabolite mimicry. The lead compound, FKK6, binds directly to PXR protein in solution, induces PXR specific target gene expression in, cells, human organoids, and mice. FKK6 significantly represses pro-inflammatory cytokine production cells and abrogates inflammation in humanized mice. The development of FKK6 demonstrates for the first time that microbial metabolite mimicry is a viable strategy for drug discovery and opens the door to mine underexploited regions of chemical space.

Introduction

Microbial metabolite mimicry has been proposed as a means to probe areas of chemical space that have been previously underexploited for drug or probe discovery [1]. However, to-date, there has been no critical proof of this concept with regards to new drug discovery for treatment of human disease.

Our laboratory had previously demonstrated that bacterial metabolism of L-tryptophan results in the formation of indoles and indole-derived metabolites, such as indole 3-propionic acid (IPA), which are effective ligands for both mouse and human pregnane X receptors (PXR), and can regulate host small intestinal immunity *via* the Toll-Like Receptor 4 (TLR4) pathway [2]. The use of PXR as a therapeutic target for inflammatory bowel disease (IBD) is a compelling concept in both rodents and humans [3]. While a variety of PXR-activating xenobiotics exist, they all have significant off-target effects in vivo (e.g., drug interactions) which limits their use as clinical drugs for IBD [4].

Using a model developed in our laboratory [2], we have shown that the co-occupancy of indole and indole 3-propionic acid (IPA) at the human PXR ligand-binding pocket and/or domain (LBD) is feasible. There are several opportunities to improve ligand binding *via* alteration of the pharmacophore H-bonding and pi-pi interactions [2]. This led us to propose that endogenous metabolite mimicry could yield more potent PXR ligands (agonists) but with limited toxicity since they would be largely derived from non-toxic metabolite-like subunits [5,6]. Further support for this concept comes from noting that basal indole levels in feces range in the low millimolar concentrations and these levels are relatively non-toxic to mammalian cells [LD_{50} oral in rats ~ 1 g/kg, ThermoFisher Scientific Safety Sheet data] [7]. Similarly, indole metabolites like IPA, in feces, are likely to be present in low to high micromolar concentrations. Indeed, while these concepts have been proposed [1], there are very few, if any, clear examples of the utility of these concepts in drug or probe discovery.

The present work was aimed at providing the requisite proof that by developing mimics of microbial indoles using limited chemical analog development, one can significantly improve binding of the indole derivatives to the receptors involved in abrogating intestinal inflammation. Several indole analogs were evaluated as specific PXR agonists and their corresponding off-target liabilities were evaluated. The safety profile of the most promising candidates was assessed in mice and human intestinal organoids in culture. Finally, the action of the PXR-specific lead compounds on intestinal inflammation in mice and human organoids was evaluated.

Results

Characterization of FKK compounds as hPXR and/or AhR agonists. Based on our novel findings that indole and IPA can synergistically activate hPXR and can produce functional effects in vivo [2], we hypothesized that the development of a small molecule, representing the interactions of both indole an IPA, is an innovative and potentially promising strategy for generating therapeutics for targeting PXR for diseases such as IBD. To design such molecules, we used our platform technology called the hybrid structure based (HSB) method. The HSB method utilized the interactions of both IPA and indole in the ligand binding domain (LBD) of PXR and the resulting pharmacophore was screened, and the molecules ranked by their individual docking score. Two commercial molecules FKK999 and BAS00641451(BAS451) (Supplementary Fig. 1a), which had docking scores of 65.89 and 52.66, respectively, were chosen as the starting point for further optimization. Docking studies demonstrated that although both FKK999 and BAS451 orient in the binding pocket of PXR to maximize their interactions with the residues from LBD, FKK999 had a better interaction profile that resembled the interactions of indole and IPA in the same site (Supplementary Fig. 1b). Docking of BAS451 shows several shared interactions with those of FKK999, but does not include the key ring stacking interaction with Trp299 and electrostatic interactions that contribute to the binding efficacy since BAS451 has only two indole rings and the additional phenyl ring does not compensate for the lost interactions. In PXR cell based transactivation screens, FKK999 activated PXR, BAS451 did not

(data not shown). FKK999 was used for further design of improved bis-indole analogs (FKK 1-10), and all analogs were tested as PXR ligands using in silico approaches (including sites outside the LBD, courtesy AC and SV). As demonstrated by the interactions of FKK5 in the LBD (Supplementary Fig. 1c) the ligand has arene-H interactions with Ser247 and Met250, electrostatic interactions with Met250 and Cys301 and other favorable interactions with Gln285, His407, Cys284, Met246 and Leu411.

The complete syntheses of indole metabolite mimics FKK1–FKK10 are reported in detail in the Supplementary Methods and Results. Crystal structures were obtained for lead compounds FKK5 (Supplementary Fig. 1d) and FKK6 (Supplementary Fig. 1e). The ligand efficiency metrics (LEM) [8] analysis [9] for the FKK compounds predicted - FKK5 and FKK6, as the best candidates for further studies (data not shown). The same LEM analysis also indicated FKK4 as an efficient agonist; however, this congener could show metabolic instability with its *N*-protecting group possibly generating toxic aldehydes by oxidative cleavage in vivo.

All compounds synthesized were tested for their potential to activate PXR and/or AhR via luciferase assays as previously described [10,11,12]. All FKK compounds demonstrate a concentration-dependent effect on PXR activation (Fig. 1a). By contrast, only FKK2 and FKK9 at 10 μM, respectively, demonstrated significant (>100 fold) AhR activation comparable with dioxin (TCDD) control ligand. To a much lesser extent, variable degrees of dose dependent AhR activation profiles were observed for FKK3,4,7,8,10 and FKK999 (Figure 1b). FKK compounds did not activate glucocorticoid receptor (GR) (Supplementary Fig. 2a), vitamin D receptor (VDR) (Supplementary Fig. 2b), thyroid receptor (TR) (Supplementary Fig. 2c) and androgen receptor (AR) (Supplementary Fig. 2d) using cell-based luciferase assays previously described [13,14]. Similarly, FKK5 or 6 did not induce constitutive androstane receptor (CAR) activity (Supplementary Fig. 2e). Since RXR is an obligatory protein partner in the active PXR transcription complex, we also assessed the potential for FKK compounds

to serve as ligands for RXR [15]. Employing a recently developed radio-ligand binding assay for RXR [16], using nuclear extracts from rat liver, we only observed significant displacement of [^{3}H]-9-*cis*-retinoic acid by FKK1, and to a lesser extent by FKK8 (Supplementary Fig. 2f). Together, molecular docking, LEM analysis, PXR and AhR transactivation assays show that among the FKK compounds, FKK5 and FKK6 are the best chemical PXR specific ligand leads.

Characterization of FKK Compound(s) Gene Expression Assay Profile in Cells. PXR agonists transcriptionally induce (> 2-fold) canonical target genes encoding drug metabolism enzymes/transporter, *CYP3A4* and *MDR1*, in both liver (hepatocytes) [17] and intestinal cells (LS180) [18]. HepaRG cells simulate hepatocytes in that PXR ligands can also induce target genes in similar but not identical manner [19-21]. AhR agonists transcriptionally induce target genes, *CYP1A1* and *CYP1A2*, in both hepatocytes [22] and intestinal cells (LS180) [23]. As shown in Fig. 1c (top panel), in LS180 cells, FKK5 and FKK6, respectively, did not induce CYP1A1 mRNA. In PXR-transfected LS180 cells, FKK6 (and to a lesser extent FKK5), induce CYP3A4 (Fig. 1c middle panel) and MDR1 mRNA (Fig. 1c, bottom panel). In HepaRG cells harboring loss of PXR or AhR, target gene induction should be markedly diminished when compared to the wild type control cell line [24,25]. TCDD, a known AhR ligand, induces CYP1A1 mRNA in HepaRG™ control 5F clone and PXR-KO cells. FKK5 and FKK6 did not induce CYP1A1 mRNA (Fig. 1c, top panel). Rifampicin, a canonical PXR ligand, did not induce CYP3A4 mRNA in HepaRG™ PXR-KO cells as compared with HepaRG™ control 5F clone or HepaRG™ AhR-KO cells. FKK6 > FKK5, respectively, induce CYP3A4 mRNA only in HepaRG™ control 5F clone or HepaRG™ AhR-KO cells (Fig. 1c, middle panel). By contrast, and unlike in LS180 cells, none of the compounds, including rifampicin, induced MDR1 mRNA (Fig. 1c, bottom panel). In primary human hepatocytes (plated, *n* = 4 independent samples), TCDD induced CYP1A1 mRNA in all hepatocytes. FKK5 and FKK6 did not induce CYP1A1 mRNA (Fig. 1c, top panel). Rifampicin and FKK6, unlike FKK5, showed >2fold induction in one of four hepatocyte samples (Fig. 1c, middle

panel). Similarly, FKK6, but not FKK5, showed MDR1 mRNA induction in one of four hepatocyte samples (Fig. 1c, bottom panel).

In comparing the PXR target gene expression profile between cell-based models (Fig. 1c), there is a greater induction of CYP3A4 and MDR1 mRNA in LS180 cells when compared with HepaRG cells or primary human hepatocytes.

Characterization of FKK Compound(s) Cell and tissue Cytotoxicity Potential. LS180 were used to assess cell cytotoxicity using the MTT assay as previously described [13,14]. The results show that the entire series of FKK compounds (up to 10 μM) do not significantly alter LS180 cell survival (Supplementary Fig. 3a). Since in vitro cytotoxicity studies do not reflect in vivo effects of metabolites as would be generated from FKK compounds in vivo (animals), an acute toxicity study was conducted in C57BL/6 mice. FKK6 was selected as a lead compound for assessment, given that it had the more favorable PXR-selective ligand activity in cell lines tested. A dose of 500 μM in 10% DMSO [26,27] per day was chosen since this concentration represented the maximal solubility of FKK6 in an aqueous solution that could be safely administered to mice. The mice were gavaged for ten (10) consecutive days and necropsied on day 12 with collection of blood (serum). FKK6 does not alter serum chemistry profiles assessed (Supplementary Fig. 3b). FKK6 does not significantly impact tissue pathology when compared to control (vehicle) exposed mice (Supplementary Table 3). Similarly, a 30-day toxicity test was conducted in mice using FKK6 at an oral dose of 200 μM in 0.8% DMSO per day. This dose was chosen to stay within the safe DMSO dose administered to mice over a 30-day period. On day 30, mice were necropsied with collection of blood (serum). FKK6 does not significantly alter serum chemistry profiles (Supplementary Fig. 3c and d) or impact tissue pathology when compared to control (vehicle) exposed mice (Supplementary Table 4).

Characterization of FKK-induced PXR – DNA interactions via Chromatin Immunoprecipitation (ChIP). To determine if FKK5 and 6 are able to enhance occupancy of specific PXR DNA-binding

elements (PXRE) in cells, we performed ChIP assays using LS174T cells transiently transfected with a PXR expressing plasmid. Extensively passaged LS174T cells endogenously express PXR but at low levels insufficient for good PXR protein pull-down and reporter experiments [28]. Thus, PXR transfection allows us to confidently isolate PXR occupancy effects in response to ligands. We verified a semi-quantitative ChIP using PXR-transfected LS174T cells exposed to FKK6 or its vehicle (DMSO). FKK6 augments PXR occupancy of the proximal CYP3A4 and MDR1 promoter (at their respective, PXR-binding elements) (Fig. 1d).

Characterization of FKK 5 and 6 as direct ligands of PXR in solution. PXR activation is repressed via kinase-dependent phosphorylation (e.g., cdk2) [29]. FKK5 and FKK6 (DiscoverX *scan*MAX^{SM} assay panel of 468 kinases) were tested as potential inhibitors of kinases in vitro and neither of these compounds inhibits the kinases tested (Supplementary Fig. 4a & Table 5). Together, these results support a direct interaction of FKK compounds with PXR. To demonstrate this interaction, we performed a cell-free competitive hPXR TR-FRET binding assay. In this assay, FKK5 demonstrated an IC_{50} of 3.77 μM which was similar to that observed with FKK6 ~ 1.56 μM (Fig. 1e). To obtain direct proof of interaction with hPXR LBD, we performed isothermal titration calorimetry (ITC) experiments using His-tagged hPXR LBD protein (PXR.1) in solution. ITC measures the affinity, K_a, and Gibbs energy ($\Delta G = -RTlnK_a$) and the changes in enthalpy, ΔH, and entropy, ΔS, associated with the binding of the FKK compounds ($\Delta G = -RTlnK_a = \Delta H - T\Delta S$). Enthalpic and entropic contributions to binding affinity define the nature of the forces that drive the binding reaction [30,31]. This information is conveyed in a thermodynamic signature [32,33] and guides drug design and optimization [34]. In agreement with previously demonstrated work that IPA alone has weak hPXR LBD interactions as determined using cell based assays [2], in this assay, unlike rifampicin, a canonical hPXR agonist , IPA does not induce a thermal signature with respect to its interaction with the hPXR LBD in solution (Supplementary Fig. 4b). FKK5 binds to a single site in LBD, albeit with better affinity than IPA (K_d = 0.30 μM) due to a more favorable enthalpy of binding (ΔH = –2.5 kcal/mol, –TΔS = –6.4 kcal/mol)

(Fig. 1f). Compared to FKK5, FKK6 binds with improved enthalpy (ΔH = -–3.5 kcal/mol) but with an even larger loss in favorable entropy ($-T\Delta S$ = –4.1kcal/mol), which translates to a loss in binding affinity for FKK6 (K_d = 2.7 μM) (Fig. 1f).

In addition, we have previously shown that unlike rifampicin, indole in combination with IPA, is unable to activate the PXR mutant (C285I/C301A) [2]. Similarly, to test the effect FKK6 (10 μM) on this mutant, 293T cells were transfected with wild-type PXR.1 or mutant PXR.1 (C285I/C301A) plasmids along with its cognate luciferase reporter. The cells were exposed to DMSO, rifampicin (10 μM) or FKK6 (10 μM) and reporter activity assessed. While rifampicin significantly induces PXR reporter activity in both wild-type and mutant PXR transfected cells, FKK6 is unable to activate mutant PXR (Fig. 2a). Together, these data show that FKK5 and FKK6 are *bonafide* agonist ligands of PXR.1 in solution and cells.

Characterization of FKK5 and FKK6 on PXR-TLR4 and NF-κB signaling in human colon cancer cells. We have previously shown that PXR activation down-regulates TLR4 mRNA expression leading to inhibition of NF-κB signaling [2,35,36]. We have also shown that FKK5 and FKK6 interact directly with PXR LBD and result in its activation. Thus, to determine the effect of FKK5 and FKK6 on the PXR-TLR4-NF-κB signaling pathway, we used PXR-transfected Caco-2 cells and exposed these cells to FKK5 and 6 since undifferentiated Caco-2 cells inherently have low PXR expression (not detected) but relatively higher TLR4 expression and are excellent in vitro models for the study of enterocyte function[36-39]. FKK5 and FKK6 down-regulates TLR4 (0.39-fold and 0.49-fold, respectively) but up-regulates CYP3A4 (3.7-fold and 3.29-fold, respectively) and MDR1 (5.12-fold and 6.45-fold, respectively) mRNA expression (Fig. 2b). Together, these studies provide a rationale for the study of FKK compounds on modulating the PXR-TLR4-NF-κB pathway.

To determine whether FKK5 and 6 also inhibit NF-κB signaling in intestinal cells, we used PXR and NF-κB reporter co-transfected as well as NF-κB reporter transfected LS180 intestinal cell line in early

and late passage. In this assay, the enhanced expression of PXR protein was verified by immunoblotting across several repeat experiments (Supplementary Fig. 4c). FKK5 and FKK6, in a dose-dependent manner, significantly reduced TNFα-induced NF-κB reporter activity in PXR-un-transfected and transfected LS180 cells (Fig. 2c). The effects of FKK compounds on inhibition of TNFα-induced NF-κB reporter activity are significantly greater in PXR-transfected cells as compared with un-transfected LS180 cells (Fig. 2c). Notably, the trend for effects of FKK5 and FKK6 is similar across the passages of LS180 cell lines used (Fig. 2c & d). Notably, PXR-transfected LS180 cells induce PXR target genes (CYP3A4, MDR1) well above un-transfected cells, and FKK5 and FKK6 induce PXR target gene expression in the transfected LS180 cells (Supplementary Fig. 4d).

To reproduce these findings in a more robust model, we used LS174T cells, in which PXR protein is absent, via a CRISPR-Cas9 knockout of the human PXR locus (see methods). Since the LS174T PXR knockout cells (*PXR*-KO or *NR1I2* KO) were pooled transfectants, the editing efficiency being ~ 83%, we see that these cells can gain some functional PXR activity with multiple passages (Supplementary Fig. 5a) even though the PXR protein expression remains very low to undetectable (Supplementary Fig. 5b). FKK 5 and FKK6 do not induce PXR target genes in *PXR*-KO cells (Supplementary Fig. 5c). In early passage *PXR*-KO cells, we used PXR and NF-κB reporter co-transfected as well as NF-κB reporter-transfected *PXR*-KO cell line. However, we were unable to see sustained PXR protein in the PXR transiently transfected *PXR*-KO cells (data not shown); thus, rather than perform the complementation experiment, we proceeded with establishing the effect of rifampicin and FKK6 in the TNF-exposed *PXR*-KO cell line transfected with the NF-κB reporter. Unlike the wild-type LS174T cells, neither rifampicin nor FKK6 repressed NF-κB reporter activity (Fig. 2e). Together, these data confirm that FKK5 and FKK6 are agonist ligands of PXR and that their activity in varied intestinal cells on repressing the TLR4 - TNF-α - NF-κB is directly via PXR.

Characterization of FKK5 and FKK6 in human colon cancer cells and intestinal organoids exposed to inflammatory and infectious stimuli. To further characterize the anti-inflammatory

effects of FKK5 and 6 on human intestinal cells and tissue, we first determined their effects on Caco-2 cell monolayers. These cells were well-established models to study intestinal cell differentiation and physiology, specifically under conditions of inflammatory stimuli [38]. Differentiated Caco-2 cells via long term culture have heightened PXR expression [40]. In Caco-2 cells, interleukin-8 (IL8) rather than IL6 is consistently a more robust pro-inflammatory cytokine (data not shown). In these cells, TNF-α significantly induced IL8 mRNA; however, only FKK6 (25 μM) significantly reduced cytokine-induced IL8 (Fig. 3a). Interestingly, cytokines (when compared to untreated cells) also significantly increased salmonella invasion in Caco-2 cells (Fig. 3b). FKK5 and 6, at all concentrations tested (10 and 25 μM), when compared to cytokines only, significantly decreased cytokine-induced salmonella invasion (Fig. 3b). There is no significant effect of FKK5 or 6 alone on salmonella invasion (Fig. 3b). Similarly, in Caco-2 cells, NF-κB is a seminal regulator of both IL8 and other pro-inflammatory cytokines. In Caco-2 cells, at 2 or 12 h, cytokines (CK only) translocate most of the NF-κB signal by immunofluorescence from the cytoplasm to the nucleus (when compared to No CK) (Fig. 3c). In the presence of FKK5 or 6 (25 μM, respectively), however, there is increased cytoplasmic NF-κB signal, suggesting more retention of NF-κB outside the nucleus (Fig. 3c).

While Caco-2 cultures are important models to study intestinal barrier function, they have limitations in that culture conditions can widely change the experimental results [39]. Thus, for a more accurate representation of the effects of compounds on PXR activity, especially with regards to inflammation, we investigated the effects of our FKK analogs on primary human intestinal organoids (HIOs). First, we confirmed that our analogs, FKK5 and 6, significantly induce PXR target genes (Supplementary Fig. 6a). Interestingly, CYP3A4, a target gene that is only modestly (as opposed to MDR1) elevated in our intestinal cell lines exposed to FKK5 (Fig. 1c), was also only modestly increased in the HIO experiments (Supplemental Fig. 6a: borderline significance for CYP3A4 $p = 0.056$). Since HIOs can be used to study effects of FKK compounds on PXR target genes, to determine if this would correlate with their ability to inhibit TNFα mediated induction of pro-inflammatory cytokine (IL8), HIOs from

different individuals were exposed to TNFα in the presence or absence of FKK5 (n = 9) or FKK6 (n = 3) or FKK9 (n = 5). In pair-wise comparison of HIOs from the same individual exposed to DMSO or FKK compounds, respectively, FKK5 (10 μM) significantly lowered IL8 mRNA levels (Figure 4a); similarly, FKK6 (10 μM) reduced IL8 mRNA levels in organoids but did not reach statistical significance (p = 0.07) (Figure 4b). FKK9, which is a strong AhR agonist but also has PXR agonist activity, did not show significant effects on IL-8 mRNA levels in this assay (Figure 4c). Complementing this data, in iPSC derived HIOs, cytokines induce a significant increase in IL8 mRNA levels at 12 h (Figure 3d; $p < 0.05$ Two Way ANOVA) but not at 2 h after exposure. FKK5 and FKK6 (each at 10 and 25μM, respectively), has no significant effect on basal IL8 expression (Figure 3d); however, when compared to cytokines alone, in the presence of cytokines both FKK5 and 6 significantly reduced IL8 mRNA expression after 12 h of exposure (Figure 3d). Similarly, cytokines significantly increased salmonella invasion in HIOs (Figure 3e). FKK5 and FKK6 (both at 10 and 25 μM, respectively), had no significant effect on basal levels of salmonella invasion (Figure 3e); however, when compared with cytokines alone, FKK5 and FKK6, both significantly reduced salmonella invasion (Fig. 3e). Interestingly, salmonella invasion is significantly reduced at all time-points studied (2, 4, 6 and 12 h post exposure to cytokines). In HIOs, at 2 or 12 h, by visual inspection of the immunofluorescence images, cytokines (CK only) translocated most of the NF-κB signal from the cytoplasm to the nucleus (CK+FKK compared to No CK) (Fig. 3f). In the presence of FKK 5 or 6 (25 μM, respectively), however, there was increased cytoplasmic NF-κB signal, suggesting more retention of NF-κB outside the nucleus (Fig. 3f).

Together, these data in Caco-2 cells, HIOs derived from multiple sources and centers, suggest that the lead FKK compounds, FKK5 and 6, are capable of inducing PXR target gene expression in all intestinal cell types. This correlates with reduction of TNFα induced pro-inflammatory cytokine (IL8) expression, reduced invasion from intestinal pathobiont, *S. typhimurium* as well as reduced accumulation of nuclear NF-κB.

PXR target gene expression in mice. The FKK compounds presented here are first generation indole/IPA analogs that have not been optimized for pharmaceutical discovery. However, to determine the effects in vivo, specifically as it relates to the ability to induce PXR target genes in different mice tissues after oral gavage, we performed studies using FKK6, our representative best lead, in C57BL/6 mice. FKK6 was gavaged at concentration ~ 500 μM in 10% DMSO and administered to C57BL/6 mice over 36 or 60 h (3 or 5 doses, respectively). There was no significant effect (< 2-fold induction with large variability) in PXR target gene (cyp3a11, mdr1a, mdr1b or mdr1) expression across organs (liver, small and large intestine) in mice (Fig. 4d: 36 h; Supplementary Fig. 6b: 60 h). There is a borderline induction of cyp3a11 (2.07-fold) in the large intestine of wild-type mice (Supplementary Fig. 6b). In *pxr* $^{-/-}$ mice exposed to FKK6, the expression levels for all target genes (cyp3a11, mdr1) are ≤ 1.5fold to that of DMSO exposed mice. Indeed, there is no biologically significant effect on PXR target gene (mdr1) expression across organs (liver, small and large intestine) in *pxr* $^{-/-}$ mice (Fig. 4e: 36 h; Supplementary Fig. 6c: 60 h). However, cyp3a11 is significantly suppressed in the small (0.25x DMSO) and large intestines (0.36x DMSO) in the 60 h exposure study (Supplementary Fig. 6c). These data suggest that PXR might be important in these organs as basal regulators of these genes. By contrast, there is a biologically significant induction of cyp3a11 (but not mdr1) expression in small and large intestines as compared to DMSO and/or liver cyp3a11 expression in *hPXR* mice when exposed to 36 h of FKK6 (three doses) (Fig. 4f). Interestingly, when the FKK6 dosing is prolonged (five doses or 60 h exposure), there is a distinct increase in mdr1 expression in the liver (as compared to the intestines) and no significant effects on cyp3a11 expression in *hPXR* mice (Supplementary Fig. 6d). Together, these results demonstrate that FKK compounds induce PXR target genes in a PXR-dependent manner in mice.

Effect of FKK6 in mouse model of acute colitis in vitro and in vivo. To characterize the effects of lead compound, FKK6, on murine colitis, adult C57Bl/6 female *hPXR* mice were exposed to DSS acutely. Mice either received once daily vehicle gavage plus intrarectal bolus or FKK6 (200 μM) oral

gavage plus intrarectal bolus (200 μM) for 10 days until necropsy. FKK6 treated mice showed significantly less weight loss and significantly greater colon length on day 10 (Figure 5a, b). The inflammation score was significantly less for FKK6 treated mice (Figure 5c); however, the fecal lipocalin 2 and FITC-dextran measurements show a decreased trend only (Figure 5d, e). These findings are replicated when we use the clustering method (weight loss, colon length), wherein it correctly identifies the two groups of mice that received two different treatments. By including, fecal lipocalin 2 as a cluster feature in the analysis then the clustering method identifies the two groups of mice correctly except for one of the samples. By contrast, FKK6 did not alter weight loss, colon length, inflammation score, lipocalin 2 or FITC-dextran levels in *pxr* $^{-/-}$ mice (Figure 6f–j). Together, these results show that a representative FKK lead compound, FKK6, significantly reduces dextran sodium sulfate (DSS) induced colitis in mice in a PXR-dependent manner.

Discussion

A longstanding problem in drug design and discovery is the very limited regions of chemical space that are exploited by the molecules conventionally available to small and large pharmaceuticals and academia. While it has been proposed that natural metabolite derivatives are likely to serve as more potent and well tolerated drugs, proof of this concept is lacking [1]. Herein, we show that indole compounds of the FKK series mimic the docking of the natural indole and indole propionic acid derivatives for PXR, and have produced two potent lead compounds, FKK5 and FKK6. While not optimized for therapeutic delivery, these leads showed significant activity in suppressing intestinal inflammation in vitro and, for FKK6, in mice and human tissues simulating colitis.

There are several caveats to bear in mind when evaluating the data presented. While we show direct binding of FKK6 to PXR protein, our studies have not resolved the direct binding residues that interact with FKK6. Ongoing research to obtain a crystal structure of co-crystallized PXR and FKK is currently

underway. The in vivo disposition of FKK compounds and their metabolites is currently unknown. The importance of pharmacokinetic profiling is that it will allow us to partially explain the serendipitous results that our FKK compounds lack PXR activation properties in liver cells (primary hepatocytes and HepaRG), as compared with intestinal cells (LS180, LS174T). The metabolites generated in mice may also have importance, in that they could inhibit parent compound interactions with PXR, and these will be studied further. Recent research reveals that intestinal PXR activators can induce hypertriglyceridemia and metabolic perturbations [41]. We did not observe any significant changes in lipid profiles in mice exposed to either a 10-day or 30-day gavage of FKK6. Indeed, it is likely that one explanation for this might be that PXR activation can have opposing effects on lipid metabolism depending on the nature of the xenobiotic itself (i.e. non-receptor mediated action of the compound itself like anti-oxidant function) [42]. These effects may cancel out on certain pathways like lipid metabolism [42]. FKK6 has been studied with respect to a limited number of cellular targets that relate to PXR. While we find that FKK effects in cells and human intestinal organoids (HIOs) correlates with changes in PXR target gene and NF-κB signaling, it is possible that some of its protective effects could come via other targets hitherto uncharacterized (e.g., tubulin) [43]. Loss of PXR studies in HIOs would be required to confirm these correlations; these studies are in progress using both LS174T cells and iPSC cells in which PXR is knocked out using CRISPR-Cas9. We have shown that FKK6 has utility in the DSS-induced model of colitis. The use of mouse models beyond DSS induced colitis (e.g., *IL10*$^{-/-}$) could broaden the translatability of these compounds during preclinical drug development. Future strategies to improve solubility and targeted delivery could include formulations used in existing compounds for colon targeted delivery [44]. Despite these caveats, our studies provide and validate the initial proof-of-concept of the utility of microbial metabolite mimicry as a potential drug discovery modality.

In summary, the FKK lead compounds are suitable starting points for further optimization of potency and/or for improving drug-like qualities and similar properties for preclinical drug discovery. The

applications would be in fields in which deficiency in intestinal permeability alters (worsens) disease manifestations (e.g., inflammatory bowel disease) [45]. Additionally, since these are relatively well tolerated agents, applications in chemoprevention are also possible. Our work describes the first fully realized drug discovery using microbial metabolite mimicry. These strategies could be expanded widely to other receptors (and diseases) that derive ligands from the host microbiome.

EXPERIMENTAL SECTION (Online Methods)

Chemistry, Compound Crystal structure, LEM analysis and In silico experiments. See *Supplementary Methods*

Biology. Rifampicin, 2,3,7,8 – tetrachlorodibenzo-*p*-dioxin (TCDD), dexamethasone, 1α,25 Dihydroxyvitamin D_3, Triiodo- L-Thyronine (T3), Dihydrotestosterone (DHT), SR12813 (S4194) were purchased from Sigma. LS174T cells were originally purchased from ATCC and prior to use cell line authenticity and was validated as previously described [46]. Caco-2 cells were purchased from ATCC and was validated by multiplexed STR DNA profiling performed by Genetica. Human Caucasian colon adenocarcinoma cells LS180 (ECACC No. 87021202) were purchased from European Collection of Cell Cultures (ECACC). Stably transfected gene reporter cell lines AZ-AHR, AZ-GR, IZ-VDRE, PZ-TR and AIZ-AR were as described elsewhere [12-14,47,48]. Cells were cultured in Dulbecco's modified Eagle's medium (DMEM) or RPMI-1640 medium (cultivation of AIZ-AR cells) supplemented with 10% of fetal bovine serum, 100 U/mL streptomycin, 100 mg/mL penicillin, 4 mM L-glutamine, 1% non-essential amino acids, and 1 mM sodium pyruvate. Cells were maintained at 37 °C and 5% CO2 in a humidified incubator. HepaRG™ is a human hepatoma cell line isolated from a liver tumor of a female patient suffering from hepatocarcinoma and hepatitis C infection [49]. The cells possess a pseudodiploid karyotype and have been characterized as an oval duct bi-potent hepatic cell line as

they have the ability to differentiate into both biliary and hepatocyte lineages in the presence of DMSO[50]. Three HepaRG™ derived cell lines, including 5F Clone control cells, and cells with targeted functional PXR and AhR gene knockouts, PXR-KO and AhR-KO respectively, were purchased from Sigma (CZ). Cells were handled according to the manufacturer´s protocol. Human Hepatocytes were purchased from Biopredic International (France) and Triangle Research Labs, LLC-Lonza (US). Cultures were maintained in serum-free medium at 37 °C and 5% CO_2 in a humidified incubator.

Generation of PXR knockout LS174T cell line. LS174T cells (ATCC: CL-188; 7 000 3535) (Synthego Corporation, Redwood City, CA) were the parental cells used to generate pooled clones of PXR knockout. CRISPR Cas9 mediated knockout cell (pool/clone) of (gene name) in (cell line) cells were generated by Synthego Corporation (Redwood City, CA, USA). Briefly, cells were first tested negative for mycoplasma. Guide RNA was selected for high activity, specificity and activity to create premature stop codons through frameshift mutations in the coding region via insertions and or deletions (Indels)within exon 2 of the gene encoding human *PXR* (*NR1I2* transcript ID ENST00000337940). To generate specific guide RNAs, based on off-target analysis, the following modified RNAs were selected - *NR1I2 -119,807,249 5' AAGAGGCCCAGAAGCAAACC-3' [TGG]-PAM*. To generate these cells, ribonucleoproteins (RNPs) containing the Cas9 protein and synthetic chemically modified sgRNA (Synthego) were electroporated into the cells using Synthego's optimized protocol. Editing efficiency is assessed upon recovery, 48 h post electroporation. Genomic DNA is extracted from a portion of the cells, PCR amplified and sequenced using Sanger sequencing. The resulting chromatograms are processed using Synthego Inference of CRISPR edits software (ice.synthego.com). The pooled PXR KO clones were validated for PXR protein (loss of) expression and target gene induction activity through serial passages (Supplementary Fig. 5a & b).

Cell Culture and Transfection Assays. Cells were seeded in 96 well plates, stabilized for 24 h, and then incubated for 24 h with tested compounds; vehicle was DMSO (0.1 % v/v). Incubations were

performed in four technical replicates. LS180 cells transiently transfected by lipofection (FuGENE HD Transfection Reagent) with pSG5-PXR plasmid along with a luciferase reporter plasmid p3A4-luc[10,11], were used for assessment of PXR transcriptional activity. Transcriptional activity of AHR, GR, VDR, TR and AR were studied in stably transfected gene reporter cell lines AZ-AHR, AZ-GR, IZ-VDRE, PZ-TR and AIZ-AR, respectively [12-14,47,48]. Cells were seeded in 96-well plates, stabilized for 24 h, and then incubated for 24 h with tested compound and/or vehicle DMSO (0.1% v/v) in the presence (antagonist mode) or absence (agonist mode) of rifampicin (RIF; 10 μM), 2,3,7,8-tetrachlorodibenzo-*p*-dioxin (TCDD; 5 nM), dexamethasone (DEX; 100 nM), calcitriol (1α,25-VD3; 50 nM), 3,5,3'-triiodothyronine (T3; 10 nM) or dihydrotestosterone (DHT; 100 nM) respectively. After the treatments, cells were lysed and luciferase activity was measured on Tecan Infinite M200 Pro plate reader (Schoeller Instruments, Prague, Czech Republic). The data are expressed as fold induction ± SD of luciferase activity over the control cells (agonistic mode — in the absence of a model ligand) or as a percentage of maximal activation ± SD (antagonistic mode — in the presence of a model ligand). Differences were tested using one-way ANOVA with Dunnett's post hoc test, $p < 0.05$, was considered significant (*). For data presented in Supplementary Figure 8, transfections and analysis of AhR activation was performed as previously published [51]. For all the transfection experiments, specifically mutiplexed transfections, the control wells were mock transfected (PXR vector). However, to exclude that PXR ligand (FKK) effect is not due to the non-specific binding of PXR (or other factors) upstream of the luciferase gene within non-PXR binding elements, we performed pilot experiments in different cell passages (P11, P14, P17) of LS174T cells using a mock luciferase plasmid (luciferase not containing an upstream PXR binding element of the CYP3A4 promoter). The PXR ligands tested were rifampicin (10 μM) and FKK6 (1–25 μM). There was no effect of these ligands at any concentration on luciferase reporter activity (data not shown).

Reverse transfection assays were performed in Caco-2 cells as previously published with the following modifications [52]. The assays were performed in a 48-well plate format using 3.0×10^4 cells

per well using pSG5-PXR plasmid (300 ng/well); β-Gal expression plasmid (600 ng/well); CYP3A4-luciferase reporter (500 ng/well) as previously published [10]. Transfection using lipofectamine® LTX (1 µl/mg of plasmid) proceeded for 24 h followed by an additional 24 h exposure to FKK5. Cell lysates were prepared for β-Gal and luciferase assays as previously published [10]. The data are expressed as mean ± SD RLU (relative light units from luciferase assay) normalized to β-Gal activity in the same well. Differences were tested using 2-way ANOVA with Tukey's multiple comparison test, $p < 0.05$ was considered significant (*). Standard transient transfection assays (PXR, CAR) in HEK293T cells were performed as previously published [53].

NF-κB reporter assays were performed using LS180 cells. Briefly, LS180 cells (Passage 8 and 13 were used since NF-κB activity can be influenced by cell passage) [54] were transiently transfected using Fugene HD transfection reagent with a reporter plasmid pNL3.2-NF-κB-RE[NlucP/NF-κB-RE/hygro] from Promega (Hercules, CA, USA); with or without co-transfection of the wt-PXR expression vector. The transfected cells were seeded in 96-well plates at density 2.5×10^4 cells per well. Following 16 h of stabilization, cells were treated with a vehicle (DMSO; 0.1% v/v), rifampicin (RIF; 10 µM) or tested compounds FKK5 and/or FKK6 in a concentration range from 0.1 to 25 µM for 24 h. For the last 4 h of the treatment, a combination of tested compounds or rifampicin with tumor necrosis factor α (TNFα; 5 ng/mL), a model inducer of NF-κB receptor transcriptional activity, was applied. Following the incubation time, cells were lysed, and Nano luciferase activity was measured in 96-well format using a Tecan Infinite M200 Pro plate reader (Schoeller Instruments, Czech Republic).

Quantitative Real-Time PCR. Cells were seeded in 6-well plates, stabilized for 24 h, and then incubated for 24 h with test compounds; vehicle was DMSO (0.1% v/v). Primary human hepatocytes from four different donors (HEP200529, HEP220932, HEP200533, HEP200538) were incubated for 24 h with test compounds; vehicle was DMSO (0.1% v/v). Total RNA was isolated using TRI Reagent® (Molecular Research Center, Ohio, USA). cDNA was synthesized from 1000 ng of total

RNA using M-MuLV Reverse Transcriptase (New England Biolabs, Ipswich, Massachusetts, USA) at 42 °C for 60 min in the presence of random hexamers (New England Biolabs). Quantitative reverse transcriptase-polymerase chain reaction (qRT-PCR) was performed using LightCycler® 480 Probes Master on a LightCycler® 480 II apparatus (Roche Diagnostic Corporation). The levels of *CYP1A1, CYP1A2*, *CYP3A4, MDR1* and *GAPDH* mRNAs were determined using Universal Probes Library (UPL; Roche Diagnostic Corporation) probes and primers listed below:

Gene symbol	**Forward primer sequence**	**Reverse primer sequence**	**UPL probe No.**
CYP1A1	CCAGGCTCCAAGAGTCCA	GATCTTGGAGGTGGCTGCT	33
CYP1A2	ACAACCCTGCCAATCTCAAG	GGGAACAGACTGGGACAATG	34
CYP3A4	TGTGTTGGTGAGAAATCTGAG G	CTGTAGGCCCCAAAGACG	38
MDR1	CCTGGAGCGGTTCTACGA	TGAACATTCAGTCGCTTTATTTCT	147
GAPDH	CTCTGCTCCTCCTGTTCGAC	ACGACCAAATCCGTTGACTC	60

The following protocol was used: an activation step at 95 °C for 10 min was followed by 45 cycles of PCR (denaturation at 95 °C for 10 s; annealing with elongation at 60 °C for 30 s). The measurements were performed in triplicate. Gene expression was normalized *per GAPDH* as a housekeeping gene. The data were processed according to the comparative C_T method [55]. Data are expressed as fold induction ± SD over the vehicle-treated cells. The bar graph depicts one representative experiment of a series of experiments performed in three consecutive passages of cells. Differences were tested using one-way ANOVA with Dunnett's post hoc test, $p < 0.05$ was considered significant.

In a separate set of experiments in Caco-2 cells, 1 x 10^5 cells were transfected with pSG5-PXR in 6 well plates for 12 h, then treated with vehicle (0.1% DMSO), Rifampcin, FKK5 and FKK6 each at a concentration of 10 μM, respectively, in triplicate for 24 h. Cells were harvested for preparation of total RNA using TRIzol Reagent (ambion, #15596026, Carsbad, CA 92008) and reverse transcribed to cDNA using the High Capacity cDNA Reverse Transcription Kit (Thermo Fisher Scientific, #4368814,

LT 02241). RT-qPCR was performed using Thermo Fisher PowerUp SYBR Green Master Mix (# A25742) and Thermo Fisher qPCR 7900HT. Each sample RT-qPCR was repeated in quadruplicate and normalized to internal control, GAPDH. The entire experiment was repeated at least 2 separate times. The primer sequences are noted below.

Gene symbol	**Forward primer sequence**	**Reverse primer sequence**
CYP3A4	GGGAAGCAGAGACAGGCAAG	GAGCGTTTCATTCACACCACCA
MDR1	AAAAAGATCAACTCGTAGGAGTA	GCACAAAATACACCAACAA
TLR4	TGTGAAATCCAGACAATTGA	AAACTCTGGATGGGGTTTCCTG
GAPDH	TCTCTGCTCCTCCTGTTC	CTCCGACCTTTCACCCTTCC

Cytotoxicity Assays. For LS180 cells, the MTT colorimetric assay was performed as previously published [14,56] and using established proliferation assay kits (Vybrant MTT Cell Proliferation Assay kit, Ref # V13154, lot # 1774057, Life Technologies).

Chromatin Immunoprecipitation (ChIP) Assays. LS174T cells were plated in 150-mm cell culture dishes followed by transfection with pSG5-PXR (2 µg/plate/1 x 10^7 cells). After 12 h, cells were exposed to vehicle (DMSO 0.1% v/v) or 10 µM FKK5, FKK6 or FKK9, respectively, for 24 h. Chromatin Immunoprecipitation (ChIP) was performed using previously published protocols[46,57]. Briefly, cells were chemically cross-linked with formaldehyde in culture media for 15 min at room temperature. Glycine was added to a final concentration of 0.125 M to stop cross-linking for 5 min at room temperature. Cells were rinsed twice with cold PBS (pH 7.5) and scraped in PBS supplemented with protease inhibitor cocktail (PIC).

Cell pellets were collected and immediately resuspended in immunoprecipitation (IP) buffer (150 mM NaCl, 50 mM Tris-HCl at pH 7.5, 5 mM EDTA, 0.5% NP-40, 1% Triton X-100). The nuclei were centrifuged at 12000 x *g* for 1 min and resuspended in fresh IP buffer. Chromatin was sheared by

sonication to average size of 0.2-0.9 kb. Lysates were cleared by centrifugation at 12,000 x *g* for 10 min. Chromatin from 2 x 10^6 cells (about 200 µl) was incubated overnight at 4 °C with the following 2 µg rabbit anti-PXR (sc-25381, Santa Cruz Biotechnology, CA), or normal rabbit IgG (sc-2027, Santa Cruz Biotechnology, CA). Immune Complexes were captured with 20 µl of packed Protein A-Agarose (sc-2001, Santa Cruz Biotechnology) per IP for 1h at 4 °C and washed three times with IP buffer. Ten percent (10%) (wt/vol) Chelex 100 was added to the beads followed by boiling of the suspension and centrifugation at 12000 x *g* for 1 min to obtain chromatin.

Purified chromatin DNA was used to perform RT-qPCR. We used PowerUp SYBR Green Master Mix (A25742, Thermo Fisher Scientific, TX) in a 10 µl reaction, 0.5 µl DNA template, 0.5 µl primer pairs (10 µM each), 5 µl Master Mix and 3.5 µl H_2O in 384-well plates on an ABI 7900, default three-step method, 40 cycles. Data was analyzed using SDS 2.2.1 program (ABI Biotechnology). We used the following primers for ChIP:

CYP3A4-F 5'-ATGCCAATGGCTCCACTTGAG-3'

CYP3A4-R 5’-CTGGAGCTGCAGCCAGTAGCAG-3'.

MDR1-F 5’-ACCAACTGTTCATTGGTCTGC-3’

MDR1-R 5’-GCAATCAGCTTAGTACCTGGATG-3’.

CYP1A1-F 5’- AGCTAGGCCATGCCAAAT-3’

CYP1A1-R 5’-AAGGGTCTAGGTCTGCGTGT-3’

Expression and purification of His-tagged PXR Ligand Binding Domain (LBD) protein. The cloning, expression and purification of His-tagged PXR LBD was performed as previously published [58] with the following modifications in the stated protocol as follows. For protein expression, Luria-Bertani (LB) media was inoculated with a saturated culture of BL21-Gold cells transformed with HIS-LIC plasmid containing the PXR LBD construct. The mixture was allowed to shake at 37 °C until the cells reached an OD_{600} ~ 0.6, and then the temperature was reduced to 18 °C, at which time IPTG was added (final concentration of 0.1 mM) to induce protein expression. For purification, the His-tag was not removed, and the un-cleaved protein was loaded onto the gel filtration column with buffer containing HEPES (25 mM, pH 7.5) and NaCl (150 mM).

Isothermal titration calorimetry (ITC). Isothermal titration calorimetry (ITC) was carried out using a VP - ITC microcalorimeter from MicroCal/Malvern Instruments (Northampton, MA, USA). The protein and its ligands were prepared in 25 mM Hepes, pH 7.5, with 150 mM NaCl and DMSO at a concentration of 6% for the experiment with FKK5 and FKK6 and 2% in the experiment with rifampicin and 3-IPA. In all the experiments the ligand solution was injected in 10-μL aliquots into the calorimetric cell containing PXR-LBD (ligand binding domain) at a concentration of 3 - 6 μM. The respective concentrations of FKK5, FKK6, rifampicin, and 3-IPA in the syringe were 60, 80, 330, and 400 μM. The experiments were carried out at 37 °C. The heat evolved upon each injection of the ligands was obtained from the integral of the calorimetric signal. The heat associated with binding to PXR-LBD in the cell was obtained by subtracting the heat of dilution from the heat of reaction. The individual heats were plotted against the molar ratio, and the enthalpy change (ΔH), association constant ($K_a = 1/K_d$), and the stoichiometry were obtained by nonlinear regression of the data. In the case of rifampicin, a binding model was chosen that took into account two sets of sites with different binding affinities.

hPXR TR-FRET. The LanthaScreen TR-FRET PXR (SXR) Competitive Binding Assay Kit (PV4839; Invitrogen, USA). The PXR ligand binding assay of FKK5, FKK6, and FKK9 was performed using LanthaScreen TR-FRET PXR (SXR) Competitive Binding Assay Kit according to the manufacturer's instructions. The assays were done in a volume of 20 µl in 384-well black plates containing different concentrations of tested compounds in the range of 1 nM to 25 µM. DMSO and 100µM SR12813 were used as a negative and positive control, respectively. The reaction mixture was incubated at room temperature for 1 hour in a dark, and then fluorescent signals were measured at 495 nm and 520 nm, with the excitation filter 340 nm, on Infinite F200 microplate reader (Tecan Group Ltd, Switzerland). Finally, the TR-FRET ratio was calculated by dividing the emission signal of 520 nm by that at 495 nm. All PXR binding assays were performed as two independent experiments, each with a minimum of four replicates. Final IC_{50} were obtained by processing the data with GraphPad Prism 6 using standard curve interpolation (sigmoidal, 4PL, variable slope). Since rifampicin, at higher concentrations, interferes with FRET signals in this assay [59,60], SR12813 serves as a positive control PXR agonist ligand and it demonstrates an IC_{50} of 0.127 µM, which is similar to previously published results [60].

Human studies. Human tissues (duodenum), was collected according to standard research protocols approved by the Institutional Review Board and Department of Pathology at Cincinnati Children's Hospital (IRB: 2014-6279; renewed 11/27/2017).

Additional samples were collected from consenting healthy patients undergoing colonoscopy at the University of Calgary endoscopy unit for colon cancer screening or to investigate gastrointestinal symptoms with normal colonoscopic appearance and normal histology (Study ID: REB18-0631_REN1). Biopsies via endoscope were taken from the colonic mucosa and immediately placed in Intesticult^{tm} Organoid Growth Media supplemented with antibiotic/antimycotic (Stemcell Technologies) and transferred from the unit to the lab.

Isolation of crypts and culture of human enteroids from patient-derived duodenum (and RT-PCR assays). Discarded duodenum tissue after surgery was obtained and used to isolate crypts. Embedded crypts in Matrigel formed three-dimentional (3D) structure referred to as 'enteroids'. The isolation protocol has been described as previously [61]. Enteroids were incubated with 10 μM compounds (FKK5, FKK6, and Rifampicin) at day 4 from isolation. DMSO was added to enteroids as negative control. After incubation for 24 h, enteroids were collected in RNA-free tube followed by breaking down Matrigel by pipetting vigorously (using 1 mL PBS). The enteroids were pelleted at 16000 g for 3 min (4°C). RNA was extracted using miRNA isolation kit (Invitrogen; #AM1561) using the protocol provided by Invitrogen. The cDNA was synthesized from the extracted RNA (final amount of RNA: 1 μg) using SuperScript III (Invitrogen, #18080-051) through two-step procedure provided by Invitrogen. PowerUp SYBR Green (Applied Biosystem, #A25742) was used for RT-PCR and performed 40 cycles using Quant Studio3 (Invitrogen, #A28132).

Primers (Invitrogen, #A15612)

- ABCC2 (F): CCCTGCTGTTCGATATACCAATC
- ABCC2 (R): TCGAGAGAATCCAGAATAGGGAC
- UGT1A1 (F): CATGCTGGGAAGATACTGTTGAT
- UGT1A1 (R): GCCCGAGACTAACAAAAGACTCT
- MDR1 (F): TTGCTGCTTACATTCAGGTTTCA
- MDR1 (R): AGCCTATCTCCTGTCGCATTA
- CYP3A4 (F): AGATGCCTTTAGGTCCAATGGG
- CYP3A4 (R): GCTGGAGATAGCAATGTTCGT
- GSTA1 (F): CTGCCCGTATGTCCACCTG
- GSTA1 (R): AGCTCCTCGACGTAGTAGAGA

Culture of human-derived colonic enteroids and FKK treatment assays (Calgary Protocol). Samples were immediately processed to yield isolated colonic crypts as previously described [62]. Isolated colonic crypts were embedded in Matrigel® (Corning) and cultured in Intesticult^{tm} Organoid Growth Media. Human organoids were pretreated for 6 h with either FKK5, FKK6, FKK9 or vehicle (DMSO) in Intesticult^{tm} Organoid Growth Media. Organoids were then stimulated with human recombinant TNFalpha in the presence of either treatment for an additional 12 h. After the 12 h treatment organoids were washed in PBS, disrupted in Tri Reagent® (Sigma, Oakville, ON, CAN) and frozen at -80°C. After thawing, chloroform was added, samples were centrifuged for 15 min and the resulting aqueous phase was then added to equal volumes of 70% ethanol and further processed using the RNeasy mini kit (Qiagen). cDNA was synthesized using the Quantitect RT kit (Qiagen) according to the manufacturers' protocol. Resulting cDNA was used as a template for quantitative real-time PCR using Perfecta SYBR Green FastMix with ROX (QuantiBio). PCR and analysis were performed using a StepOne PCR system (Applied Biosystems). Gene expression was calculated relative to β-Actin expression and expressed as fold-change of control. The primers used were as follows: Human ®-Actin (NM_001101), Human CXCL8 (NM_000584)(data not reported), Human CYP3A4 (NM_001202855) and Human ABCB1 (NM_000927).

Caco2 cell cultures and iPSC derived human intestinal organoids (and RT-PCR Assays). Caco-2 cells (ATCC, Manassas, VA) passage 25–35 were maintained and expanded in culture flasks in Dulbecco's Modified Eagle Medium (DMEM) with 10 % FBS and 1 x antibiotic-antimycotic. The cells were kept in a humidified 37 °C incubator with 5% CO_2. Media was changed every 2-3 days and with regular passage 1-2 times a week. For all experiments, Caco-2 cells (5 x 10^4 cells/mL) were seeded into 12 well Transwell inserts or coverslips and cultured for 3 weeks. HIOs were generated from iPSCs as described previously[63], with some modifications. The iPSC cell line IISH1i-BM1 (WiCell., Madison, WI) was cultured on Matrigel plates to 80% confluence in mTeSR™1 medium (Stem Cell Technologies., Seattle, WA) and differentiated to endoderm using Definitive Endoderm Kit (Stem Cell

Technologies., Seattle, WA) for 4 days with daily media changes. Endoderm was then differentiated to hindgut for 5 days with the addition of FGF-4 (500 ng/mL; Peprotech., Rocky Hill, NJ) and Chir99021 (3 μM; Cayman., Ann Arbor, MI) in RPMI media supplemented with 2% FBS. Floating hindgut spheroids were collected on days 3–5 of hindgut differentiation and suspended in Matrigel beads for HIO differentiation. HIOs were maintained in WENRAS media [64] which maintains proliferation in the culture. Stock HIOs were passaged weekly by removing Matrigel with Cell Recovery Solution (Corning, NY) and mechanically breaking up organoids with pipetting. HIOs were seeded into new Matrigel beads at a 1:3 split, using WENRAS with added Rock Inhibitor Y-27632 (10 μM) and Chir99021 (3 μM; Cayman., Ann Arbor, MI) for the first two days of culture.

HIOs and Caco-2 were exposed to a pro-inflammatory cytokine cocktail (10 ng/mL IFNγ, 10 ng/mL TNFα, 50 ng/mL IL-1β) for varying time points (2 – 24 h) in combination with DMSO control or FKK5 and FKK6 compounds (10 and 25 μm). Relative mRNA levels of IL-8 and IL-6 were determined using quantitative real time PCR, with normalization to GAPDH. RNA was isolated using an RNeasy Mini Kit (Qiagen) as per the manufacturer's instructions. On column DNAse (Qiagen) was used to remove any contaminating DNA. Next, cDNA was formed using iScript cDNA Synthesis Kit (Bio-rad) and 100 ng RNA. Quantitative real-time PCR was performed with SsoAdvanced Universal SYBR Green kit (Bio-rad). The following primers were used: IL-8 Forward: ATACTCCAAACCTTTCCACCC; IL-8 Reverse: TCTGCACCCAGTTTTCCTTG; IL-6 Forward: CCACTCACCTCTTCAGAACG; IL-6 Reverse: CATCTTTGGAAGGTTCAGGTTG; GAPDH Forward: ACATCGCTCAGACACCAT; GAPDH Reverse: TGTAGTTGAGGTCAATGAAGGG. For immuno-fluorescent staining of NF-κB translocation to the cell nucleus, HIOs and Caco-2 cell monolayers were fixed in 4% formaldehyde (in 1 x PBS) overnight at 4 °C. The formaldehyde was removed by washing with 1 x PBS, and an antigen retrieval step was performed by incubating in 10 mM sodium-citrate buffer in a vegetable steamer for 20 min. The samples were then blocked with normal donkey serum (10 % in PBS with 0.3% Triton x-100) for one hour. Samples were incubated overnight with primary antibodies: rabbit anti- NF-κB p65 (1:400

dilution, Cell Signaling Technology., Danvers MA). Samples were then immersed in Alexa Fluor® 555 donkey anti-rabbit secondary antibody (Life Technologies) at a 1:500 dilution. Nuclei were stained with Hoechst 33342 (Life Technologies). The samples were then imaged using a Zeiss LSM880 Confocal/Multiphoton Upright Microscope, with 3-D image rendering using Volocity.

FKK compounds were tested for their ability to prevent *Salmonella* invasion in vitro in non-inflamed and inflamed cell cultures. Overnight cultures of *Salmonella typhimurium* 14038 were diluted to OD_{600} 0.01 and injected into with HIOs or immersed over Caco-2 monolayers for 1 hour at 37°C. The invasive ability of *Salmonella* was assessed using the gentamicin protection assay [65]. Bacterial adhesion scenarios to the Caco-2 surface were set up as described above. Non-adhered bacteria were removed by washing twice in PBS, followed by incubation with 1 mL gentamicin (150 µg/mL $^{-1}$ in DMEM) for 1 hour at 37°C to kill the adhered extracellular bacteria. Dead bacteria were removed by washing twice in PBS, followed by an incubation with 500 µl 0.1 % Triton X-100 for 15 min at 37°C to lyse the HIOs and Caco-2, and release the intracellular (invaded) bacteria. Serial fold dilutions and plating were then employed to determine CFU/mL. We normalized to total protein using Bradford Assay.

Animal Studies. FKK6 was solubilized to saturation concentrations (~ 500 µM) at room temperature in 10% DMSO. This concentration of DMSO is safe in mice, especially if administered in short course (maximum tolerated dose in mice is ~ 2.5 gm/kg/day for 35 consecutive days) [66,67]. C57BL/6J mice (Jackson Labs Stock 000664)(6 -10 weeks), *pxr* $^{-/-}$ (6 –10 weeks) [68], and humanized *(h) PXR* mice [Taconic, C57BL/6-*Nr1i2*$^{tm1(NR1I2)Arte}$ (9104, females; 9104, males), 6 -10 weeks] [69] were administered either 10% DMSO (*n* = 3) or FKK6 (*n* = 3) in either 3 doses or 5 doses, with each dose interval of 12 h. Each gavage dose volume was 100 µL. At 2–4h after the end of the scheduled dosing period, mice were sacrificed, and tissues harvested for further analysis. The mouse studies were performed three independent times over an 18-month period. All purchased mice were acclimatized in the Einstein vivarium for ~ 2 weeks before experiments commenced. All mice (n ≤ 5 per stainless steel cage and

separated by gender) were maintained on standard non-irradiated chow (LabDiet 5058, Lab Supply) and sterile water in the barrier facility observing a 12 h night/day cycle. The room temperature was maintained at 25 ± 2°C with 55 ± 5% humidity. All studies were approved by the Institute of Animal Studies at the Albert Einstein College of Medicine, INC (IACUC # 20160706, 20160701 and preceding protocols) and specific animal protocols were also approved by additional protocols (IACUC# 20170406, 20170504) and Animal Care and Use Review Office (ACURO) of the US Army Medical Research and Materiel Command (PR160167, W81XWH-17-1-0479).

Dextran Sulfate Sodium (DSS)-induced acute colitis studies. For these studies 7-8 week old female [70] *hPXR* and *pxr* $^{-/-}$ mice (C57Bl/6 background) were bred and each genotype was separated into two treatment groups using a random allocation method via coin toss – (1) control (vehicle treated consisting 0.8% DMSO in 100 μL drinking water) administered once per day via oral gavage and via intrarectal gavage for a total of 10 consecutive days (*n* = 3) and (2) FKK6 in 0.8% DMSO at 200 μM in 100 μL drinking water administered once per day via oral gavage and via intrarectal gavage for a total of 10 consecutive days (*n* = 3). Intrarectal delivery, at a 45° angle, was achieved using a 1 mL syringe attached to a19G needle that had a polyethylene tubing (#427516, 0.58 mm O.D, Becton Dickinson, Sparks, MD) inserted to 3 cm into anal opening under very light anesthesia (1.5% isofluorane with nose cone) till no visible liquid was seen outside the anus. Fecal pellets were collected prior to initiation of the treatment protocol. All mice were first given their treatment allocation and 4 h later were all treated with 3% DSS (MPBio LLC, Salon, OH; Cat# 160110) in drinking water. All mice were starved overnight (12 h) to allow for smooth intrarectal delivery; however, the mice were allowed to feed *ad libitum* during the day. This protocol was continued for 10 consecutive days after which mice were sacrificed and organs/tissues/feces harvested for further study. On day 10, prior to necropsy, mice were administered FITC-dextran and mouse serum was collected for the FITC-dextran assay as previously described [71]. The experimenter was not blinded to treatment allocation; however, the pathologist (KS) evaluating histologic scores is blinded to treatment allocation. All

studies were approved by the Institute of Animal Studies at the Albert Einstein College of Medicine, INC (IACUC # 20160706 and preceding protocols). Colitis scoring was performed as previously published and post-examination masking was conducted [72,73].

Statistical Analysis. All data sets were initially visually inspected and then assessed for normality and lognormality, descriptive and outlier analysis using tests specified in GraphPad Prism 8.2.0 (272) (except as noted). Student *t*-test, one-way analysis of variance (1-Way ANOVA), two-way analysis of variance (2-Way ANOVA) followed by Dunnett test, as well as values of EC_{50} and IC_{50}, was calculated using GraphPad Prism version 8.2.0 (272) for Windows (GraphPad Software, La Jolla, California, USA) are indicated as appropriate in each figure legend. The statistical analysis of FKK6 treatment end-points (% weight loss, colon length, lipocalin 2, and FITC-dextran) in *pxr*$^{+/+}$ and *pxr*$^{-/-}$ was performed using student *t*-test and non-parametric tests for non-normal data as well as by clustering clustering method on the six sample data vector to split the mice into two groups. The "kmeans" function of the R software was used to obtain the clusters.

AUTHOR INFORMATION

Corresponding Author(s)

** Email: Sridhar.mani@einstein.yu.edu Phone : (718) 430-2871 Fax: (718) 430-8550

**Email: Sandhya.Kortagere@drexelmed.edu Phone: (215) 991-8135 Fax: (215) 848-2271

**Email: moulin@email.cz Phone: + 420 585634903 Fax: n/a

Present Addresses

$ Present Address: St. Edmund's College, Shillong, Old Jowai Road, Shillong, Meghalaya 793003, India

Author Contributions

The manuscript was written through contributions of all authors. All authors have given approval to the final version of the manuscript.

‡These authors contributed equally to this work.

Additional Information (Competing Interests)

The studies presented here are included in a patent submitted by The Albert Einstein College of Medicine in conjunction with Palacký University and The Drexel University College of Medicine to the US Patent and Trademark Office. Funding for these studies are listed under acknowledgement.

ACKNOWLEDGMENTS

The studies presented here were funded in part by the ICTR Pilot Award (AECOM to S.M & F.K); Grant# 362520 Broad Medical Research Program (BMRP, not Litwin) at CCFA (Crohn's & Colitis Foundation of America) (to S.M); NIH grants R35 ES028244 (to G.H.P); CA127231; CA 161879 and Department of Defense Partnering PI (W81XWH-17-1-0479; PR160167) (to S.M.), (ES030197) (to S.M.,J.C.,H.G) as well as R43DK105694 (PI: Jay Wrobel), P30DK041296 (PI: Alan Wolkoff) (Pilot Awards, S.M); Diabetes Research Center Grant (P30 DK020541); Cancer Center Grant (P30CA013330 PI: David Goldman); 1S10OD019961-01 NIH Instrument Award (PI: John Condeelis); LTQ Orbitrap Velos Mass Spectrometer System (1S10RR029398); and NIH CTSA (1 UL1 TR001073). Additional invaluable assistance was obtained from Vera DesMarais PhD (Light Microscopy and Image Analysis Analytical Imaging Facility (AIF) Albert Einstein College of Medicine, Bronx, NY), Amanda Beck DVM (Histology and Comparative Pathology Core, Albert Einstein College of Medicine, Bronx, NY), Lars Nordstroem PhD and Chamini Karunaratne PhD (Chemical Synthesis and Biology Core, Albert Einstein College of Medicine, Bronx, NY), Yungping Qiu PhD (Stable Isotopes and Metabolomics Core Facility, Albert Einstein College of Medicine, Bronx, NY), and the Proteomics Core Facility, Albert Einstein College of Medicine, Bronx, NY, and The Czech Science Foundation [19-00236S] and the Operational Programme Research, Development and Education - European Regional Development Fund, the Ministry of Education, Youth and Sports of the Czech Republic [CZ.02.1.01/0.0/0.0/16_019/0000754](Z.D.), and Christian Jobin (*E. coli* NC101 strains, University of Florida, Gainesville, FL). Arpan De performed the biofilm assays. MMC and GL are indebted to professor Cele Abad-Zapatero who invented AtlasCBS and disclosed its potential as a tool to facilitate drug design and development endeavors. SV and AC are supported by the National Academy of Sciences, India. The authors thank Ms. Gurmeet Bindra in the inflammatory intestinal tissue bank (IITB) and the staff at the University of Calgary endoscopy unit for assistance with research sample collection and Dr. Marilyn Gordon of the Human Tissue Research Lab at the University of Calgary for sample preparation and human intestinal organoid protocol optimization. Invaluable input into the design of the clinical study and conduct and use of mouse models and for use in future IBD models was provided by Dr. Balfour Sartor via the CCFA.

ABBREVIATIONS USED

PXR, Pregnane X Receptor; SXR, steroid and xenobiotic receptor; FKK, Felix Kopp Kortagere; DMSO, dimethyl sulfoxide; AhR, aryl hydrocarbon receptor; GR, glucocorticoid receptor; VDR, vitamin D receptor; VDRE, VDR elements (DNA binding); TR, thyroid receptor; AR, androgen receptor; RT, reverse transcription; qPCR, quantitative polymerase chain reaction; TLR4, toll-like receptor 4; GLP-1, glucagon-like peptide -1; IPA, Indole 3-propionic acid; Å, angstrom; TCDD, 2,3,7,8 – tetrachlorodibenzo-*p*-dioxin; T3, Triiodo-L-Thyronine; DHT, Dihydrotestosterone; KO, knockout; 1α,25-VD3, calcitriol; DEX, dexamethasone; ADMET, absorption, distribution, metabolism, excretion, toxicology; STR, short tandem repeats; DNA, deoxyribonucleic acid; rpm, revolutions per minute; NaCl, sodium chloride; HEPES, 4-(2-hydroxyethyl)-1-piperazineethanesulfonic acid; EDTA, ethylenediaminetetra acetic acid; SDS–PAGE, sodium dodecyl sulfate polyacrylamide gel electrophoresis; CZ, Czech Republic; US, United States of America; PBS, Phosphate Buffered Saline; PIC, protease inhibitor cocktail; x *g* times gravity; MTT, 3-(4,5-dimethylthiazolyl-2)-2,5-diphenyltetrazolium bromide)

Main Figures

Fig. 1

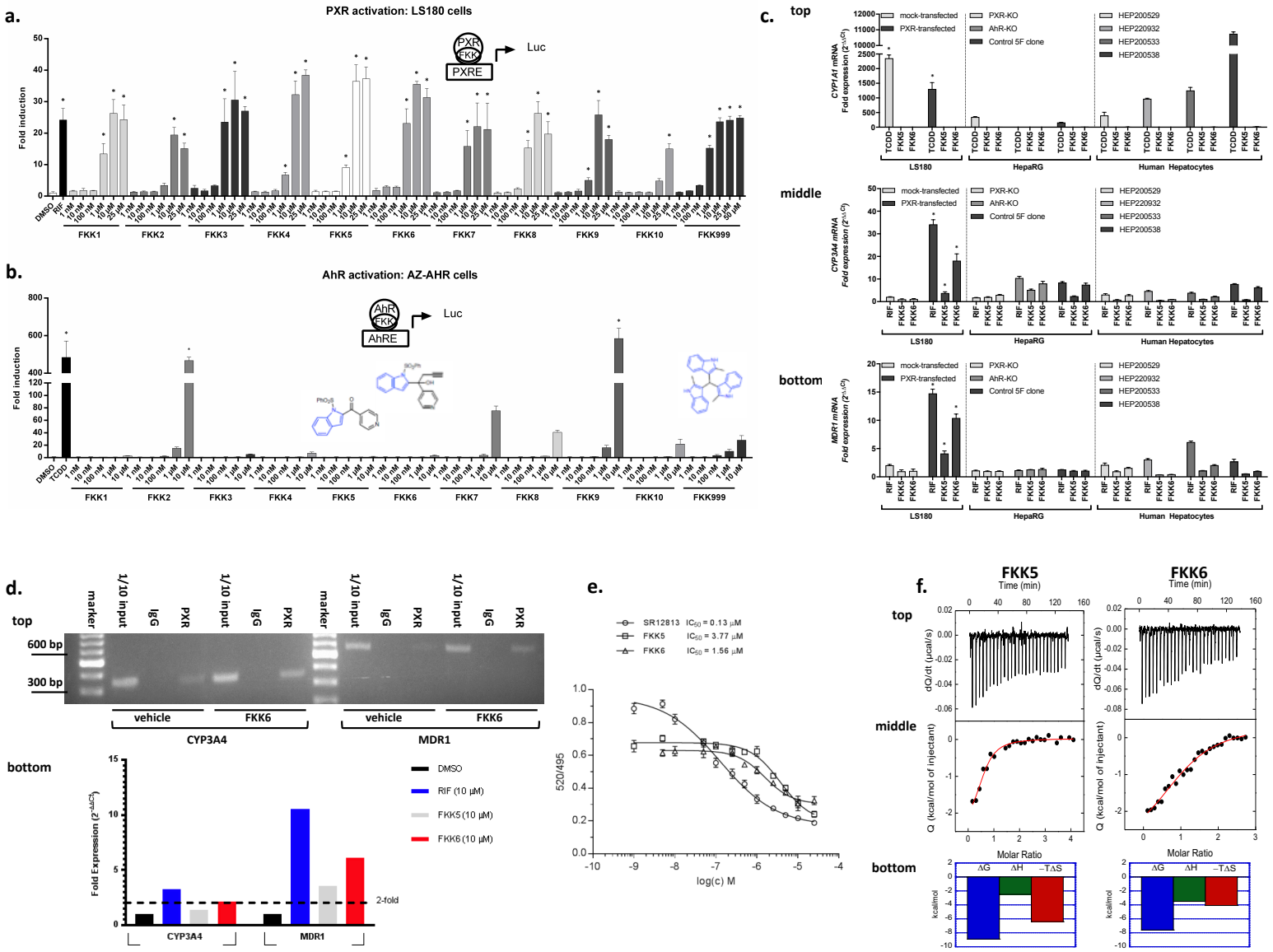

Fig. 1: FKK5 and FKK6 activate PXR. a, Histogram (mean, 95 %CI) of fold induction of PXR activity reporter assay (luc, luciferase) in LS180 cells transiently transfected with wild-type PXR and p3A4-luc reporter plasmids. **b**, same as **a**, in HepG2 cells stably expressing pCYP1A1 luciferase plasmid (AhR reporter). Chemical structures of FKK5, FKK6 and FKK999 compounds are overlaid. Indole is colored blue. **a, b,** The bar graph(s) depicts one representative experiment of a series of experiments ($n > 3$) performed in four consecutive passages of cells. Histogram (mean, 95 %CI) of fold mRNA expression, of **c**, CYP1A1 (top panel), CYP3A4 (middle panel) and MDR1 (bottom panel) in LS180 cells with or without (mock) transfected PXR plasmid, HepaRG hepatic progenitor cells (PXR-knockout, PXR-KO; AhR-knockout, AhR-KO; parental control 5F clone) and primary human hepatocytes (HEP) from four donors is shown. The bar graph represents one experiment of a series of experiments ($n > 3$) performed in four consecutive passages of LS180 cells; $n = 2$ independent experiments with one well/compound and RT-PCR performed in triplicate for each HepaRG genotype; for each donor hepatocyte, $n = 1$ well/compound and RT-PCR performed in triplicate. **d**, Chromatin Immunoprecipitation (ChIP) assay in LS174T cells. Top panel, PCR products cells exposed to vehicle or FKK6 and run on a 2% agarose gel. DNA 100 base pair marker; Vehicle,10% DMSO; FKK6 (10 μM); 1/10 Input - 0.2 million cells before IP; IgG - IP with polyclonal rabbit IgG; PXR - IP with PXR antibody. Bottom panel, quantitative PCR from the ChIP assay for compounds tested with the gene specific PCR amplicon normalized to GAPDH (fold expression). Dash line, 2-fold expression. The data is one representative experiment of two independent experiments (each $n = 3$ biologic replicates, $n = 4$ technical replicates). **e**, PXR TR-FRET assay. TR-FRET ratio 520/495 nm are plotted against concentration of compound(s). Half-maximal inhibitory concentrations IC_{50} were obtained from interpolated standard curves (sigmoidal, 4PL, variable slope); error bars show standard deviation of $n = 2$ independent experiments each with four technical replicates. **f**, Microcalorimetric titrations of PXR ligand binding domain (LBD) with FKK5 and FKK6. A single-site binding model was used for fitting the data. The upper panel shows the output signal, dQ/dt, as a function of time. The middle panel shows

the integrated heats as a function of the ligand/PXR molar ratio in the cell. The solid line represents the best non-linear least-squares fit of the data. The lower panel shows respective thermodynamic signatures of binding to the PXR ligand binding domain. *$p < 0.05$, one way ANOVA with Dunnett's post hoc test.

Fig. 2

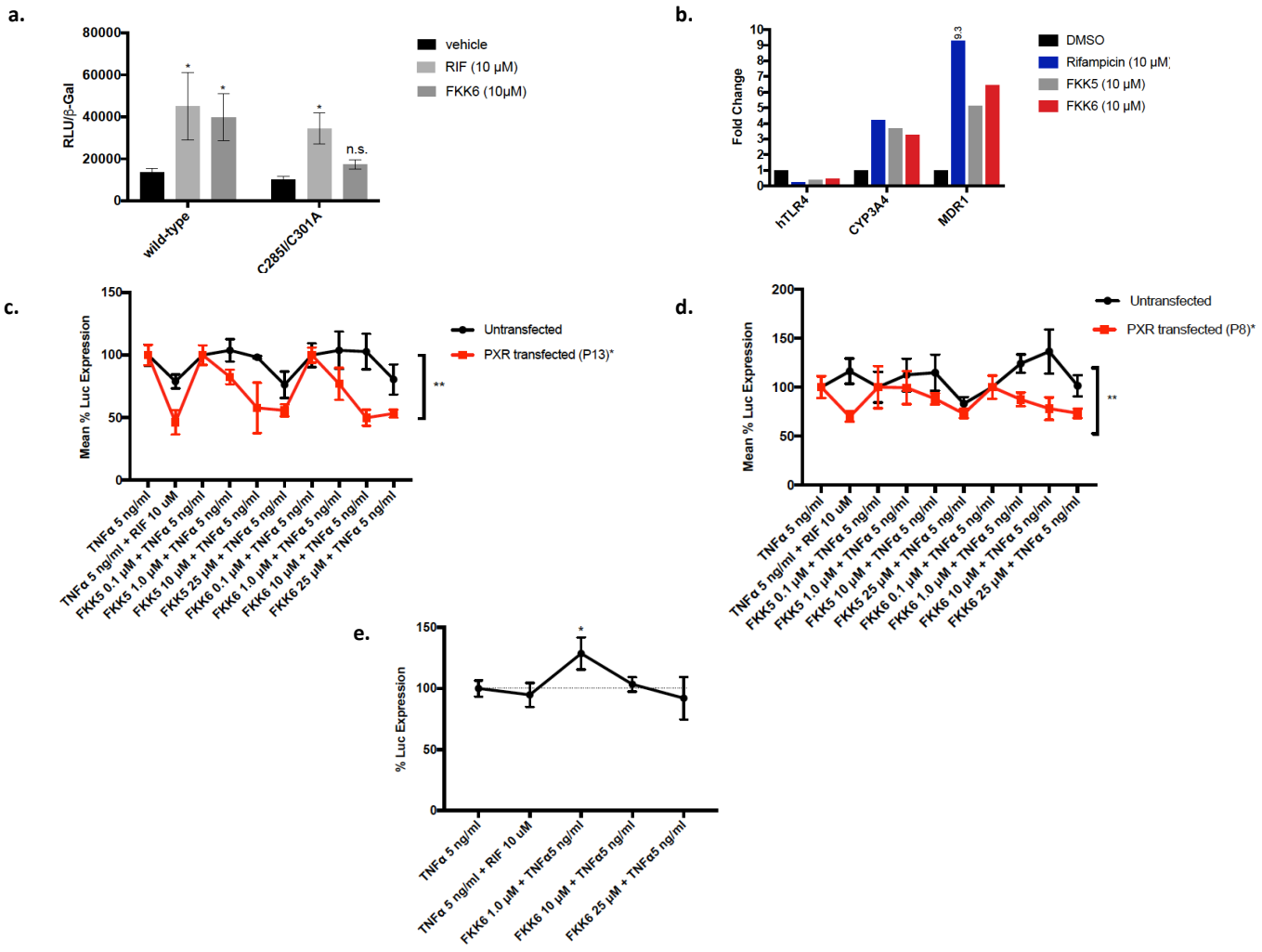

Fig. 2: FKK5 and FKK6 inhibit NF-κB activation in a PXR-dependent manner. a, PXR (luciferase) reporter assay in HEK293T cells transiently transfected with PXR plasmids (wild-type and ligand binding domain mutant C285I/C301A). RLU, relative light units are shown normalized to beta-galactosidase (β-Gal) expression. The histogram represents one experimental data (of $n > 2$ independent experiments each performed in quadruplicate) mean (95 %CI); n.s. not significant; * $p < 0.05$, two-way ANOVA. **b**, Histogram represents fold change in mRNA expression, normalized to GAPDH, by RT-qPCR from Caco-2 cells exposed to compounds. DMSO, 0.1% DMSO vehicle; 9.3 is 9.3-fold expression. The data is one representative experiment of two independent experiments (each $n = 3$ biologic replicates, $n = 4$ technical replicates). Points and error represent mean (95 %CI) values for control (TNFα 5 ng/ml) normalized NF-κB (luciferase) reporter activity in LS180 cells after **c**, Passage 13 (P13) and **d**, Passage 8 (P8) and in **e**, LS174T PXR-KO cells transiently transfected with pNL3.2.NF-κB-RE vector. **c**, **d,** Line graph depicts one representative experiment of a series of experiments ($n > 4$) performed in four consecutive passages of cells. Data was expressed as mean with 95% CI of four technical replicates. **e**, mean (± SD). *, ** $p < 0.05$, two way ANOVA with Tukey's multiple comparisons test.

Fig. 3

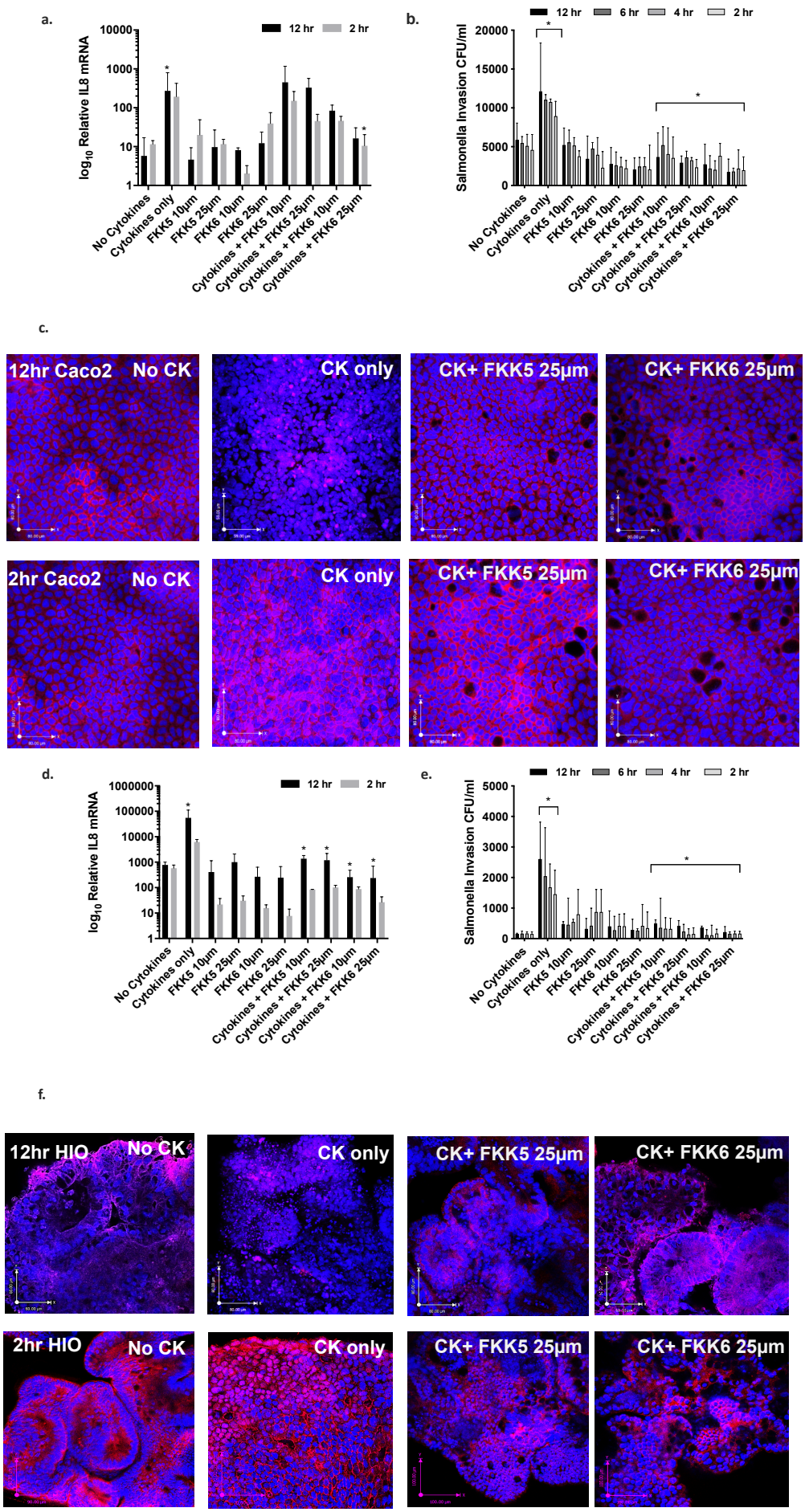
a.
12 hr
2 hr
log10 Relative IL8 mRNA
10000
1000
100
10
1
No Cytokines
Cytokines only
FKK5 10µm
FKK5 25µm
FKK6 10µm
FKK6 25µm
Cytokines + FKK5 10µm
Cytokines + FKK5 25µm
Cytokines + FKK6 10µm
Cytokines + FKK6 25µm
b.
12 hr
6 hr
4 hr
2 hr
Salmonella Invasion CFU/ml
20000
15000
10000
5000
0
c.
12hr Caco2
No CK
CK only
CK+ FKK5 25µm
CK+ FKK6 25µm
2hr Caco2
No CK
CK only
CK+ FKK5 25µm
CK+ FKK6 25µm
d.
12 hr
2 hr
log10 Relative IL8 mRNA
1000000
100000
10000
1000
100
10
1
e.
12 hr
6 hr
4 hr
2 hr
Salmonella Invasion CFU/ml
5000
4000
3000
2000
1000
0
f.
12hr HIO
No CK
CK only
CK+ FKK5 25µm
CK+ FKK6 25µm
2hr HIO
No CK
CK only
CK+ FKK5 25µm
CK+ FKK6 25µm

Fig. 3: FKK5 and FKK6 inhibit cytokine and salmonella infection induced NF-κB nuclear translocation. In Caco-2 monolayer cells **a**, Log_{10} relative expression of IL8 mRNA with or without cytokines (50 ng/ml IL-1, 10 ng/ml IFNγ, 10 ng/ml TNF α), and cytokine cocktail plus FKK drugs (10 and 25 μM) with 2 h or 12 h incubations. **b**, Salmonella invasion in colony forming units per ml (CFU/ml) at the different time periods of incubation. **c**, confocal images of NFκB (red) and the nucleus (blue). In human intestinal organoids (HIO), **d-f** are identical to **a-b**. The histogram, mean with 95% CI, depicts combined data from biological replicates (n = 3) with three consecutive passages of cells. Each biological replicate has three technical replicates. Results were expressed as. * $p < 0.05$, two-way ANOVA with Tukey post hoc test. Confocal images shown are representative images from (n = 3) biological replicates.

Fig. 4

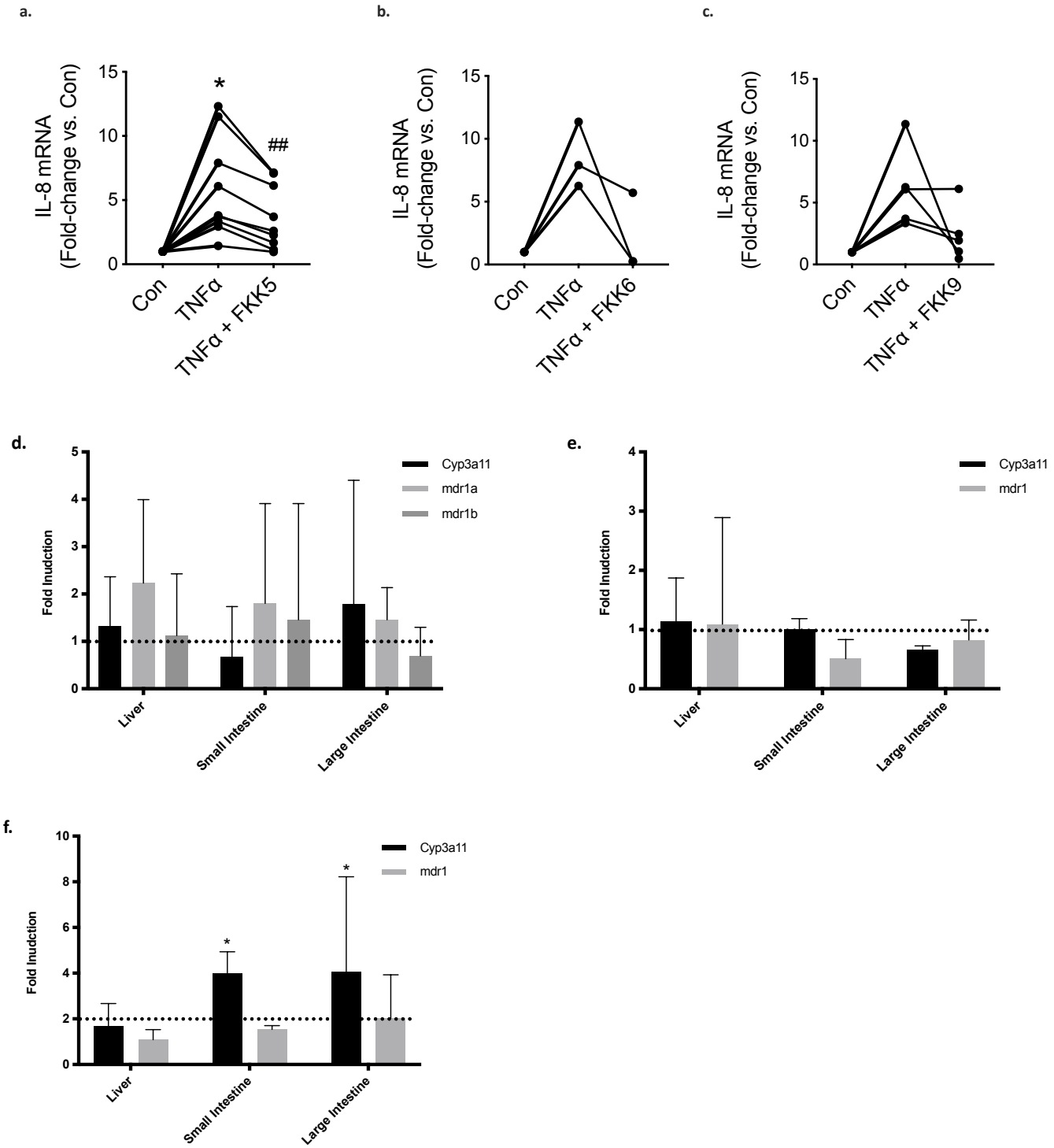

Fig. 4: FKK6 inhibits cytokine mediated IL8 induction in human colonic organoids and induces PXR target genes in mice. Quantitative gene expression by RT-qPCR of IL8 mRNA from human colonic enteroids (over 40 enteroids per individual sample per well) exposed to control (vehicle) or TNF α. with or without **a**, FKK5. **b**, FKK6. **c**, FKK9. Data shown as mean fold change relative to vehicle control (con) for each paired sample (n = 3 replicates). Each paired sample data set represents biopsies from an individual patient. *, $^{\#\#}p < 0.05$, Pair-wise one way ANOVA with Tukey's post hoc test. Fold induction (mRNA) of genes in **d**, C57BL/6 mice, **e**, *pxr* $^{-/-}$ mice, and **f**, *hPXR* mice gavaged with vehicle (10% DMSO; n = 3) or FKK6 (500 μM in 10% DMSO; n = 3) every 12h for 3 total doses. The entire experiment was repeated two independent times and one representative experiment is shown. Each mouse (each organ) was studied in quadruplicate assays and normalized to internal control, GAPDH. The histograms show mean (95% CI) values for gene expression. * $p < 0.05$, two-way ANOVA with Tukey's post hoc test.

Fig. 5

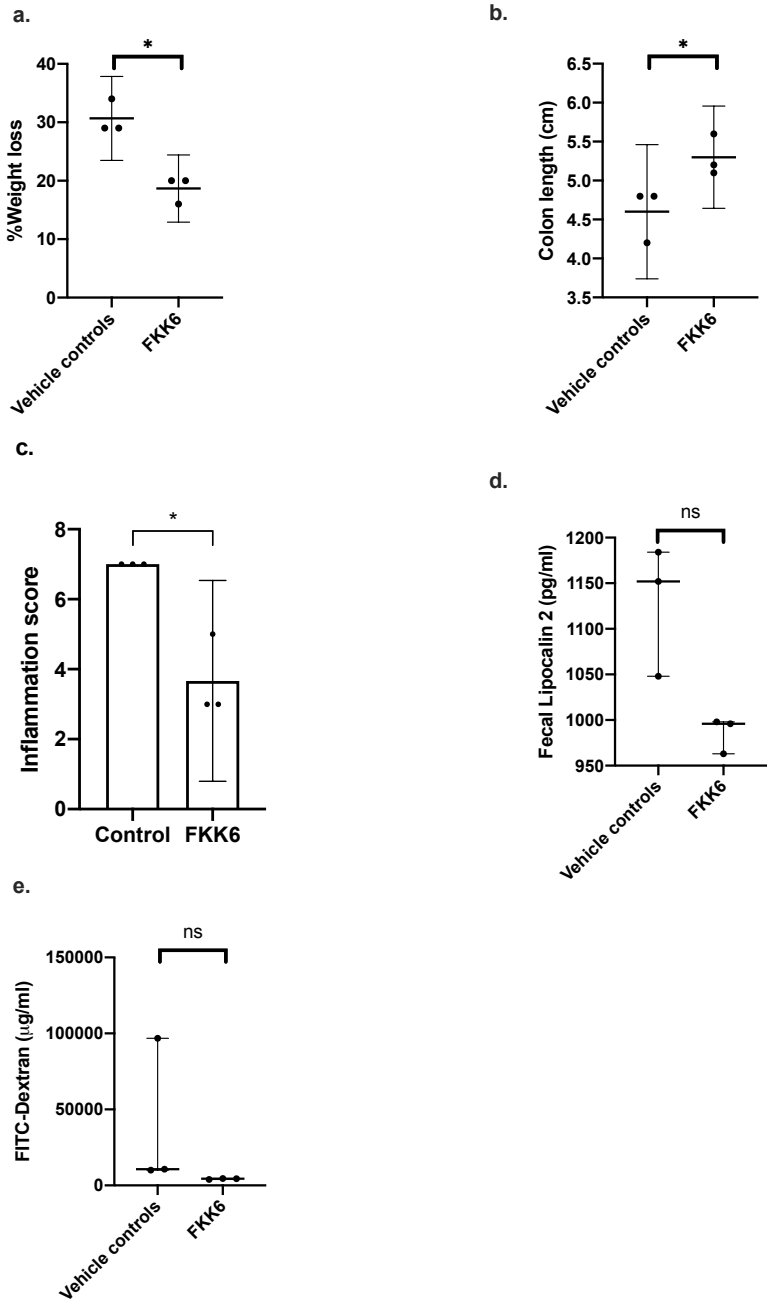

Fig. 5: FKK6 abrogates Dextran Sulfate Sodium induced colitis in humanized (h) PXR mice. After coin-toss randomization, *hPXR* mice were allocated to treatment with vehicle (0.8% DMSO) (n = 3/genotype) or FKK6 (200 micromolar) (n = 3/genotype), by simultaneous oral gavage and intra-rectal delivery starting day 1 - 10 of DSS administration. **a,** % weight loss from baseline (day 1 *vs* day 10) **b**, colon length (cm) **c**, Inflammation score (see methods) **d**, Fecal lipocalin 2 (pg/ml) **e**, serum FITC-dextran (μg/ml). **a - c**, mean (95 %CI). **d**,**e,** median (interquartile range). The entire experiment was repeated two independent times and one representative experiment is shown. *(**a**, **b**, **c**) $p < 0.05$, Welch's t-test ; *(**d**, **e**) $p < 0.05$, Mann-Whitney test; ns, not significant.

Fig. 6

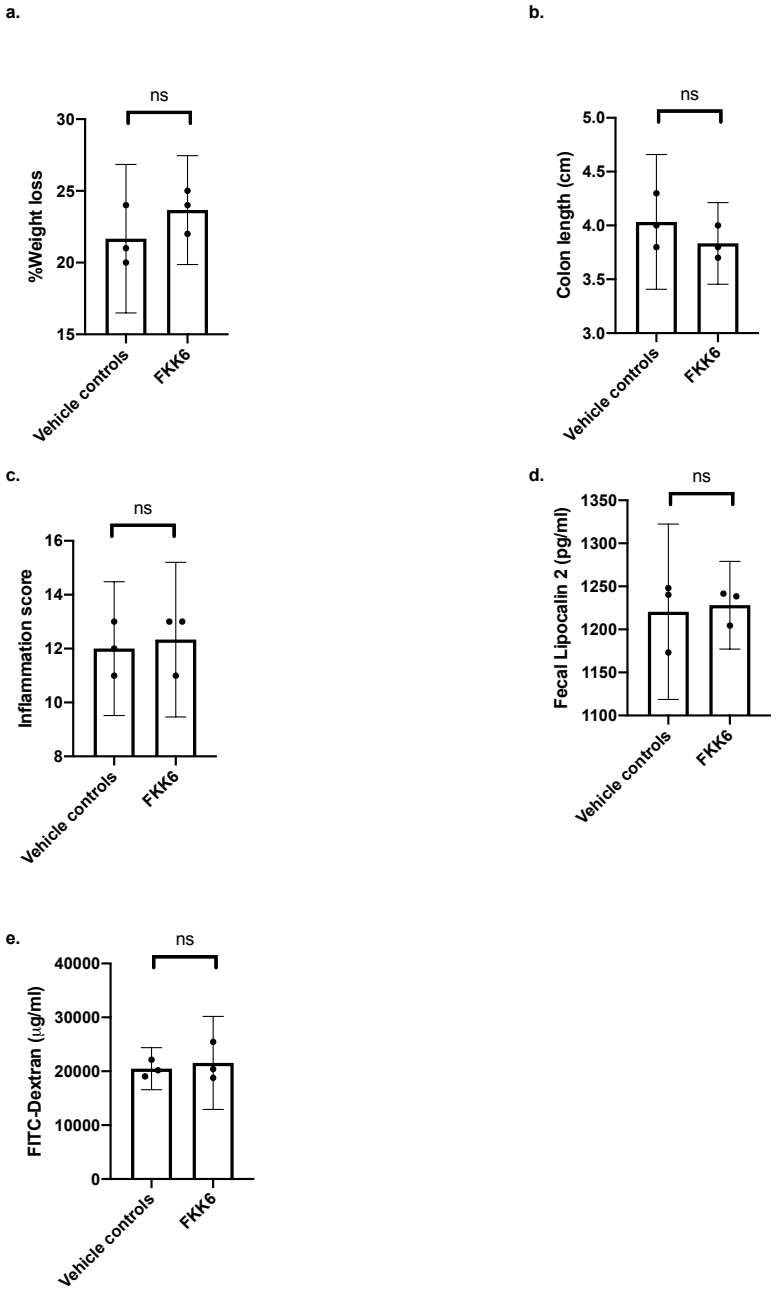

Fig. 6: FKK6 does not abrogate Dextran Sulfate Sodium induced colitis in *pxr* $^{-/-}$ mice. As in Fig 5, p*xr* $^{-/-}$ mice underwent the identical experimental procedure and analysis. The entire experiment was repeated two independent times and one representative experiment is shown. *(**a - e**) mean (95 %CI); Welch's t-test; ns, not significant.

REFERENCES

1 Saha, S., Rajpal, D. K. & Brown, J. R. Human microbial metabolites as a source of new drugs. *Drug discovery today* **21**, 692-698, doi:10.1016/j.drudis.2016.02.009 (2016).

2 Venkatesh, M. *et al.* Symbiotic bacterial metabolites regulate gastrointestinal barrier function via the xenobiotic sensor PXR and Toll-like receptor 4. *Immunity* **41**, 296-310, doi:10.1016/j.immuni.2014.06.014 (2014).

3 Cheng, J., Shah, Y. M. & Gonzalez, F. J. Pregnane X receptor as a target for treatment of inflammatory bowel disorders. *Trends in pharmacological sciences* **33**, 323-330, doi:10.1016/j.tips.2012.03.003 (2012).

4 Cheng, J., Krausz, K. W., Tanaka, N. & Gonzalez, F. J. Chronic exposure to rifaximin causes hepatic steatosis in pregnane X receptor-humanized mice. *Toxicological sciences : an official journal of the Society of Toxicology* **129**, 456-468, doi:10.1093/toxsci/kfs211 (2012).

5 Brave, M., Lukin, D. J. & Mani, S. Microbial control of intestinal innate immunity. *Oncotarget* **6**, 19962-19963, doi:10.18632/oncotarget.4780 (2015).

6 Mani, S. Indole microbial metabolites: expanding and translating target(s). *Oncotarget* **8**, 52014-52015, doi:10.18632/oncotarget.19443 (2017).

7 Chappell, C. L. *et al.* Fecal Indole as a Biomarker of Susceptibility to Cryptosporidium Infection. *Infection and Immunity* **84**, 2299-2306, doi:10.1128/IAI.00336-16 (2016).

8 Cavalluzzi, M. M., Mangiatordi, G. F., Nicolotti, O. & Lentini, G. Ligand efficiency metrics in drug discovery: the pros and cons from a practical perspective. *Expert opinion on drug discovery* **12**, 1087-1104, doi:10.1080/17460441.2017.1365056 (2017).

9 Abad-Zapatero, C. & Blasi, D. Ligand Efficiency Indices (LEIs): More than a Simple Efficiency Yardstick. *Molecular informatics* **30**, 122-132, doi:10.1002/minf.201000161 (2011).

10 Huang, H. *et al.* Inhibition of drug metabolism by blocking the activation of nuclear receptors by ketoconazole. *Oncogene* **26**, 258-268, doi:10.1038/sj.onc.1209788 (2007).

11 Goodwin, B., Hodgson, E. & Liddle, C. The orphan human pregnane X receptor mediates the transcriptional activation of CYP3A4 by rifampicin through a distal enhancer module. *Mol Pharmacol* **56**, 1329-1339 (1999).

12 Novotna, A., Pavek, P. & Dvorak, Z. Novel stably transfected gene reporter human hepatoma cell line for assessment of aryl hydrocarbon receptor transcriptional activity: construction and characterization. *Environmental science & technology* **45**, 10133-10139, doi:10.1021/es2029334 (2011).

13 Bartonkova, I., Grycova, A. & Dvorak, Z. Profiling of Vitamin D Metabolic Intermediates toward VDR Using Novel Stable Gene Reporter Cell Lines IZ-VDRE and IZ-CYP24. *Chemical research in toxicology* **29**, 1211-1222, doi:10.1021/acs.chemrestox.6b00170 (2016).

14 Bartonkova, I., Novotna, A. & Dvorak, Z. Novel stably transfected human reporter cell line AIZ-AR as a tool for an assessment of human androgen receptor transcriptional activity. *PloS one* **10**, e0121316, doi:10.1371/journal.pone.0121316 (2015).

15 Xie, W. *et al.* Reciprocal activation of xenobiotic response genes by nuclear receptors SXR/PXR and CAR. *Genes Dev* **14**, 3014-3023 (2000).

16 Toporova, L., Macejova, D. & Brtko, J. Radioligand binding assay for accurate determination of nuclear retinoid X receptors: A case of triorganotin endocrine disrupting ligands. *Toxicology letters* **254**, 32-36, doi:10.1016/j.toxlet.2016.05.005 (2016).

17 Kandel, B. A. *et al.* Genomewide comparison of the inducible transcriptomes of nuclear receptors CAR, PXR and PPARalpha in primary human hepatocytes. *Biochimica et biophysica acta* **1859**, 1218-1227, doi:10.1016/j.bbagrm.2016.03.007 (2016).

18 Gupta, A., Mugundu, G. M., Desai, P. B., Thummel, K. E. & Unadkat, J. D. Intestinal human colon adenocarcinoma cell line LS180 is an excellent model to study pregnane X receptor, but not constitutive androstane receptor, mediated CYP3A4 and multidrug resistance transporter 1 induction: studies with anti-human immunodeficiency virus protease inhibitors. *Drug metabolism and disposition: the biological fate of chemicals* **36**, 1172-1180, doi:10.1124/dmd.107.018689 (2008).
19 Aninat, C. *et al.* Expression of cytochromes P450, conjugating enzymes and nuclear receptors in human hepatoma HepaRG cells. *Drug metabolism and disposition: the biological fate of chemicals* **34**, 75-83, doi:10.1124/dmd.105.006759 (2006).
20 Andersson, T. B. The application of HepRG cells in evaluation of cytochrome P450 induction properties of drug compounds. *Methods in molecular biology (Clifton, N.J.)* **640**, 375-387, doi:10.1007/978-1-60761-688-7_20 (2010).
21 Antherieu, S., Chesne, C., Li, R., Guguen-Guillouzo, C. & Guillouzo, A. Optimization of the HepaRG cell model for drug metabolism and toxicity studies. *Toxicology in vitro : an international journal published in association with BIBRA* **26**, 1278-1285, doi:10.1016/j.tiv.2012.05.008 (2012).
22 Pastorkova, B., Vrzalova, A., Bachleda, P. & Dvorak, Z. Hydroxystilbenes and methoxystilbenes activate human aryl hydrocarbon receptor and induce CYP1A genes in human hepatoma cells and human hepatocytes. *Food and chemical toxicology : an international journal published for the British Industrial Biological Research Association* **103**, 122-132, doi:10.1016/j.fct.2017.03.008 (2017).
23 Kubesova, K., Doricakova, A., Travnicek, Z. & Dvorak, Z. Mixed-ligand copper(II) complexes activate aryl hydrocarbon receptor AhR and induce CYP1A genes expression in human hepatocytes and human cell lines. *Toxicology letters* **255**, 24-35, doi:10.1016/j.toxlet.2016.05.014 (2016).
24 Williamson, B., Lorbeer, M., Mitchell, M. D., Brayman, T. G. & Riley, R. J. Evaluation of a novel PXR-knockout in HepaRG cells. *Pharmacology research & perspectives* **4**, e00264, doi:10.1002/prp2.264 (2016).
25 Brauze, D. *et al.* Induction of expression of aryl hydrocarbon receptor-dependent genes in human HepaRG cell line modified by shRNA and treated with beta-naphthoflavone. *Molecular and cellular biochemistry* **425**, 59-75, doi:10.1007/s11010-016-2862-3 (2017).
26 Castro, C. A., Hogan, J. B., Benson, K. A., Shehata, C. W. & Landauer, M. R. Behavioral effects of vehicles: DMSO, ethanol, Tween-20, Tween-80, and emulphor-620. *Pharmacology, biochemistry, and behavior* **50**, 521-526 (1995).
27 Caujolle, F. M. E., Caujolle, D. H., Cros, S. B. & Calvet, M.-M. J. LIMITS OF TOXIC AND TERATOGENIC TOLERANCE OF DIMETHYL SULFOXIDE. *Annals of the New York Academy of Sciences* **141**, 110-125, doi:doi:10.1111/j.1749-6632.1967.tb34871.x (1967).
28 Delfosse, V. *et al.* Synergistic activation of human pregnane X receptor by binary cocktails of pharmaceutical and environmental compounds. *Nature communications* **6**, 8089, doi:10.1038/ncomms9089 (2015).
29 Smutny, T., Mani, S. & Pavek, P. Post-translational and post-transcriptional modifications of pregnane X receptor (PXR) in regulation of the cytochrome P450 superfamily. *Current drug metabolism* **14**, 1059-1069 (2013).
30 Velazquez-Campoy, A., Todd, M. J. & Freire, E. HIV-1 protease inhibitors: enthalpic versus entropic optimization of the binding affinity. *Biochemistry* **39**, 2201-2207 (2000).
31 Ruben, A. J., Kiso, Y. & Freire, E. Overcoming roadblocks in lead optimization: a thermodynamic perspective. *Chemical biology & drug design* **67**, 2-4, doi:10.1111/j.1747-0285.2005.00314.x (2006).
32 Velazquez-Campoy, A., Kiso, Y. & Freire, E. The binding energetics of first- and second-generation HIV-1 protease inhibitors: implications for drug design. *Archives of biochemistry and biophysics* **390**, 169-175, doi:10.1006/abbi.2001.2333 (2001).
33 Freire, E. Do enthalpy and entropy distinguish first in class from best in class? *Drug discovery today* **13**, 869-874, doi:10.1016/j.drudis.2008.07.005 (2008).
34 Garbett, N. C. & Chaires, J. B. Thermodynamic studies for drug design and screening. *Expert opinion on drug discovery* **7**, 299-314, doi:10.1517/17460441.2012.666235 (2012).

35 Ranhotra, H. S. *et al.* Xenobiotic Receptor-Mediated Regulation of Intestinal Barrier Function and Innate Immunity. *Nuclear Receptor Research* **3**, 1-19, doi:10.11131/2016/101199 (2016).
36 Mani, S. in *Chromatin Signaling and Diseases* (eds Olivier Binda & Martin Ernesto Fernandez-Zapico) 423-442 (Academic Press, 2016).
37 Ranhotra, H. S. *et al.* Xenobiotic Receptor-Mediated Regulation of Intestinal Barrier Function and Innate Immunity. *Nuclear receptor research* **3**, doi:10.11131/2016/101199 (2016).
38 Hung, T. V. & Suzuki, T. Short-Chain Fatty Acids Suppress Inflammatory Reactions in Caco-2 Cells and Mouse Colons. *Journal of agricultural and food chemistry* **66**, 108-117, doi:10.1021/acs.jafc.7b04233 (2018).
39 Delie, F. & Rubas, W. A human colonic cell line sharing similarities with enterocytes as a model to examine oral absorption: advantages and limitations of the Caco-2 model. *Critical reviews in therapeutic drug carrier systems* **14**, 221-286 (1997).
40 Mani, S. in *Chromatin Signaling and Diseases* (ed Martin Ernesto Fernandez-Zapico) 423-442 (Academic Press, 2016).
41 Meng, Z. *et al.* The atypical antipsychotic quetiapine induces hyperlipidemia by activating intestinal PXR signaling. *JCI insight* **4**, doi:10.1172/jci.insight.125657 (2019).
42 Hwang, I. K. *et al.* Indole-3-propionic acid attenuates neuronal damage and oxidative stress in the ischemic hippocampus. *Journal of neuroscience research* **87**, 2126-2137, doi:10.1002/jnr.22030 (2009).
43 La Regina, G. *et al.* New Indole Tubulin Assembly Inhibitors Cause Stable Arrest of Mitotic Progression, Enhanced Stimulation of Natural Killer Cell Cytotoxic Activity, and Repression of Hedgehog-Dependent Cancer. *Journal of medicinal chemistry* **58**, 5789-5807, doi:10.1021/acs.jmedchem.5b00310 (2015).
44 Guo, Y. *et al.* Advances in Pharmaceutical Strategies Enhancing the Efficiencies of Oral Colon-Targeted Delivery Systems in Inflammatory Bowel Disease. *Molecules (Basel, Switzerland)* **23**, doi:10.3390/molecules23071622 (2018).
45 Bischoff, S. C. *et al.* Intestinal permeability--a new target for disease prevention and therapy. *BMC gastroenterology* **14**, 189, doi:10.1186/s12876-014-0189-7 (2014).
46 Wang, H. *et al.* Pregnane X receptor activation induces FGF19-dependent tumor aggressiveness in humans and mice. *The Journal of clinical investigation* **121**, 3220-3232, doi:10.1172/jci41514 (2011).
47 Illes, P., Brtko, J. & Dvorak, Z. Development and Characterization of a Human Reporter Cell Line for the Assessment of Thyroid Receptor Transcriptional Activity: A Case of Organotin Endocrine Disruptors. *Journal of agricultural and food chemistry* **63**, 7074-7083, doi:10.1021/acs.jafc.5b01519 (2015).
48 Novotna, A., Pavek, P. & Dvorak, Z. Construction and characterization of a reporter gene cell line for assessment of human glucocorticoid receptor activation. *European journal of pharmaceutical sciences : official journal of the European Federation for Pharmaceutical Sciences* **47**, 842-847, doi:10.1016/j.ejps.2012.10.003 (2012).
49 Gripon, P. *et al.* Infection of a human hepatoma cell line by hepatitis B virus. *Proceedings of the National Academy of Sciences* **99**, 15655-15660, doi:10.1073/pnas.232137699 (2002).
50 Parent, R., Marion, M. J., Furio, L., Trepo, C. & Petit, M. A. Origin and characterization of a human bipotent liver progenitor cell line. *Gastroenterology* **126**, 1147-1156 (2004).
51 Murray, I. A. *et al.* Antagonism of aryl hydrocarbon receptor signaling by 6,2',4'-trimethoxyflavone. *The Journal of pharmacology and experimental therapeutics* **332**, 135-144, doi:10.1124/jpet.109.158261 (2010).
52 Kublbeck, J., Anttila, T., Pulkkinen, J. T. & Honkakoski, P. Improved assays for xenosensor activation based on reverse transfection. *Toxicology in vitro : an international journal published in association with BIBRA* **29**, 1759-1765, doi:10.1016/j.tiv.2015.07.011 (2015).
53 Huang, H. *et al.* Inhibition of drug metabolism by blocking the activation of nuclear receptors by ketoconazole. *Oncogene* (2006).

54 Mastropietro, G., Tiscornia, I., Perelmuter, K., Astrada, S. & Bollati-Fogolin, M. HT-29 and Caco-2 reporter cell lines for functional studies of nuclear factor kappa B activation. *Mediators of inflammation* **2015**, 860534, doi:10.1155/2015/860534 (2015).
55 Schmittgen, T. D. & Livak, K. J. Analyzing real-time PCR data by the comparative C(T) method. *Nature protocols* **3**, 1101-1108 (2008).
56 Schiller, C. D., Kainz, A., Mynett, K. & Gescher, A. Assessment of viability of hepatocytes in suspension using the MTT assay. *Toxicology in vitro : an international journal published in association with BIBRA* **6**, 575-578 (1992).
57 Nelson, J. D., Denisenko, O. & Bomsztyk, K. Protocol for the fast chromatin immunoprecipitation (ChIP) method. *Nature protocols* **1**, 179-185, doi:10.1038/nprot.2006.27 (2006).
58 Wallace, B. D. *et al.* Structural and functional analysis of the human nuclear xenobiotic receptor PXR in complex with RXRalpha. *Journal of molecular biology* **425**, 2561-2577, doi:10.1016/j.jmb.2013.04.012 (2013).
59 Shukla, S. J. *et al.* Identification of clinically used drugs that activate pregnane X receptors. *Drug metabolism and disposition: the biological fate of chemicals* **39**, 151-159, doi:10.1124/dmd.110.035105 (2011).
60 Shukla, S. J. *et al.* Identification of pregnane X receptor ligands using time-resolved fluorescence resonance energy transfer and quantitative high-throughput screening. *Assay Drug Dev Technol* **7**, 143-169, doi:10.1089/adt.2009.193 (2009).
61 Mahe, M. M., Sundaram, N., Watson, C. L., Shroyer, N. F. & Helmrath, M. A. Establishment of human epithelial enteroids and colonoids from whole tissue and biopsy. *Journal of visualized experiments : JoVE*, doi:10.3791/52483 (2015).
62 Fernando, E. H. *et al.* A simple, cost-effective method for generating murine colonic 3D enteroids and 2D monolayers for studies of primary epithelial cell function. *American journal of physiology. Gastrointestinal and liver physiology* **313**, G467-g475, doi:10.1152/ajpgi.00152.2017 (2017).
63 Spence, J. R. *et al.* Directed differentiation of human pluripotent stem cells into intestinal tissue in vitro. *Nature* **470**, 105-109, doi:10.1038/nature09691 (2011).
64 Fujii, M., Matano, M., Nanki, K. & Sato, T. Efficient genetic engineering of human intestinal organoids using electroporation. *Nature protocols* **10**, 1474-1485, doi:10.1038/nprot.2015.088 (2015).
65 Gagnon, M., Zihler Berner, A., Chervet, N., Chassard, C. & Lacroix, C. Comparison of the Caco-2, HT-29 and the mucus-secreting HT29-MTX intestinal cell models to investigate Salmonella adhesion and invasion. *Journal of microbiological methods* **94**, 274-279, doi:10.1016/j.mimet.2013.06.027 (2013).
66 Caujolle, F. M., Caujolle, D. H., Cros, S. B. & Calvet, M. M. Limits of toxic and teratogenic tolerance of dimethyl sulfoxide. *Ann N Y Acad Sci* **141**, 110-126 (1967).
67 Brayton, C. F. Dimethyl sulfoxide (DMSO): a review. *The Cornell veterinarian* **76**, 61-90 (1986).
68 Staudinger, J. L. *et al.* The nuclear receptor PXR is a lithocholic acid sensor that protects against liver toxicity. *Proc Natl Acad Sci U S A* **98**, 3369-3374 (2001).
69 Scheer, N., Ross, J., Kapelyukh, Y., Rode, A. & Wolf, C. R. In vivo responses of the human and murine pregnane X receptor to dexamethasone in mice. *Drug metabolism and disposition: the biological fate of chemicals* **38**, 1046-1053, doi:10.1124/dmd.109.031872 (2010).
70 DeVoss, J. & Diehl, L. Murine models of inflammatory bowel disease (IBD): challenges of modeling human disease. *Toxicol Pathol* **42**, 99-110, doi:10.1177/0192623313509729 (2014).
71 Vetizou, M. *et al.* Anticancer immunotherapy by CTLA-4 blockade relies on the gut microbiota. *Science (New York, N.Y.)* **350**, 1079-1084, doi:10.1126/science.aad1329 (2015).
72 Meyerholz, D. K. & Beck, A. P. Principles and approaches for reproducible scoring of tissue stains in research. *Laboratory Investigation* **98**, 844-855, doi:10.1038/s41374-018-0057-0 (2018).
73 Kim, J. J., Shajib, M. S., Manocha, M. M. & Khan, W. I. Investigating intestinal inflammation in DSS-induced model of IBD. *Journal of visualized experiments : JoVE*, doi:10.3791/3678 (2012).
74 Abad-Zapatero, C. *AtlasCBS: A Graphic Tool to Map the Content of Structure-Activity Databases*. (2016).

75 Sheldrick, G. M. A short history of SHELX. *Acta crystallographica. Section A, Foundations of crystallography* **64**, 112-122, doi:10.1107/s0108767307043930 (2008).
76 Sheldrick, G. M. SHELXT - Integrated space-group and crystal-structure determination. *Acta Crystallographica Section A* **71**, 3-8, doi:10.1107/S2053273314026370 (2015).
77 Sheldrick, G. M. TWINABS. *Version 2012/1. Georg-August-Universität Göttingen, Göttingen, Germany* (2012).
78 Chandran, A. & Vishveshwara, S. Exploration of the conformational landscape in pregnane X receptor reveals a new binding pocket. *Protein science : a publication of the Protein Society* **25**, 1989-2005, doi:10.1002/pro.3012 (2016).
79 Phillips, J. C. *et al.* Scalable molecular dynamics with NAMD. *J Comput Chem* **26**, 1781-1802, doi:10.1002/jcc.20289 (2005).
80 Darden, T. A. & Pedersen, L. G. Molecular modeling: an experimental tool. *Environ Health Perspect* **101**, 410-412 (1993).
81 Bussi, G. & Parrinello, M. Accurate sampling using Langevin dynamics. *Phys Rev E Stat Nonlin Soft Matter Phys* **75**, 056707, doi:10.1103/PhysRevE.75.056707 (2007).
82 Bussi, G., Donadio, D. & Parrinello, M. Canonical sampling through velocity rescaling. *J Chem Phys* **126**, 014101, doi:10.1063/1.2408420 (2007).
83 Hoover, W. G. Canonical dynamics: Equilibrium phase-space distributions. *Phys Rev A Gen Phys* **31**, 1695-1697 (1985).
84 Nosé, S. A molecular dynamics method for simulations in the canonical ensemble. *Molecular physics* **52**, 255-268 (1984).
85 Jones, G., Willett, P. & Glen, R. C. Molecular recognition of receptor sites using a genetic algorithm with a description of desolvation. *Journal of molecular biology* **245**, 43-53 (1995).
86 Jones, G., Willett, P., Glen, R. C., Leach, A. R. & Taylor, R. Development and validation of a genetic algorithm for flexible docking. *Journal of molecular biology* **267**, 727-748, doi:10.1006/jmbi.1996.0897 (1997).
87 Laskowski, R. A. & Swindells, M. B. LigPlot+: multiple ligand-protein interaction diagrams for drug discovery. *Journal of chemical information and modeling* **51**, 2778-2786, doi:10.1021/ci200227u (2011).
88 Fabian, M. A. *et al.* A small molecule-kinase interaction map for clinical kinase inhibitors. *Nature biotechnology* **23**, 329-336, doi:10.1038/nbt1068 (2005).
89 Karaman, M. W. *et al.* A quantitative analysis of kinase inhibitor selectivity. *Nature biotechnology* **26**, 127-132, doi:10.1038/nbt1358 (2008).
90 Horiuchi, K. Y. *et al.* Assay development for histone methyltransferases. *Assay Drug Dev Technol* **11**, 227-236, doi:10.1089/adt.2012.480 (2013).

Author Contribution

SM conceptualized the idea. SM, ZD, SK, FK wrote the paper. FK, CK, LUN performed the chemical synthesis for agents used in the paper. CMC, JSK, JCM performed analyses and generated Fig. 3. ZD, AV, MS, IB, EJ, KP, BV performed analyses and generated Fig. 1a-c, e, Fig. 2, as well as supplementary Fig. 2a-d, 3a, 4c & 5a-b. HR performed analyses to validate FKK effects on PXR transfected cell lines. KSM, APN performed organoid studies in Cincinnati; KF, SH performed organoid studies in Calgary. IM and GHP performed analyses, confirmed FKK-AhR activity and critically appraised the manuscript. AS performed the ITC experiments. BW, WGW, MRR generated PXR protein in solution. HG and JYC critically evaluated the manuscript and optimized mass spectrometry detection for FKK. KS performed blinded readings for pathology on colitis experiments in mice. AB provided blinded histologic analyses for toxicology experiments. SK, SV and AC provided modeling studies for FKK compounds. MMC and GL performed LEM analyses. MN performed crystal structure analyses. AM and DW performed additional studies for external validation of FKK effects and critically helped with manuscript editing and writing. HL performed all other studies including the cell line studies, ChIP assays, and all the animal studies.